SEL-73-023

The Midlatitude Ionospheric Response to Fluctuations in Solar Activity under Low Geomagnetic Activity Conditions

by

Jose Luis Bendito

May 1973

Technical Report No. 16

Prepared under

National Aeronautics and Space Administration
Research Grant No. NGR 05-020-001

RADIOSCIENCE LABORATORY

STANFORD ELECTRONICS LABORATORIES

STANFORD UNIVERSITY • STANFORD, CALIFORNIA

SEL-73-023

THE MIDLATITUDE IONOSPHERIC RESPONSE TO FLUCTUATIONS IN SOLAR ACTIVITY UNDER LOW GEOMAGNETIC ACTIVITY CONDITIONS

by

Jose Luis Bendito

May 1973

Technical Report No. 16

Prepared under

National Aeronautics and Space Administration
Research Grant No. NGR 05-020-001

Radioscience Laboratory
Stanford Electronics Laboratories
Stanford University Stanford, California

ABSTRACT

The ionospheric response (i.e., the sensitivity and delay of the electron content) to the 270day fluctuations of solar radiation has been theoretically analyzed. In the context of the present work the sensitivity is defined as the magnitude of the electron content fluctuation for a given change in solar flux, and the delay is defined as the time-shift of the response of the electron content to fluctuations in solar flux. Both the model in which the action of neutral winds on the F-2 layer is disregarded and that in which the wind effect is included as part of a positive feedback mechanism, are studied. It is shown that the neutral winds play a dominant role in the mentioned ionospheric response. The computed delays decrease with increasing solar activity in both models. Nevertheless, when the action of neutral winds is considered the delays are larger. The experimental verification of the delays computed theoretically is only possible when two conditions are met: First, that the solar flux fluctuations exhibit sufficient amplitude, and secondly, that the first condition occur during geomagnetically quiet periods. For the level of solar activity exhibited during the year period when observations were made, a fairly good agreement was found, during the favorable period in which the two conditions mentioned were met, between the delay predicted by the model in which neutral winds are included and the experimental results. The computed sensitivities from this model have found a semiquantitative agreement with experimental results due to the presence of other effects not included in the model.

ACKNOWLEDGEMENTS

I am particularly grateful to Dr. Aldo V. da Rosa for his invaluable advice and encouragement throughout the course of this work.

I am indebted to Dr. Helio Waldman for numerous suggestions and criticisms. The discussions with Mr. Dimitri Antoniadis and Dr. Odmar Almeida are also appreciated. Mr. S.C. Hall was responsible for the collection of the data used in this study. I would like to thank Mrs. Shayne Barrom for typing this dissertation.

The constant support and attention of the Universidad de los Andes (Merida, Venezuela) made possible the realization of this work. I deeply appreciate it.

This research was supported by NASA Research Grant No. NGR 05-020-001.

TABLE OF CONTENTS

TABLES

ILLUSTRATIONS

ILLUSTRATIONS

ILLUSTRATIONS

CHAPTER 1

INTRODUCTION

One of the main processes taking place in the ionosphere is the photoionization of the neutral atmosphere by solar extreme ultraviolet radiation (EUV). Most of the early papers concerning the influence of solar radiation on the ionosphere dealt with variations of the critical frequency, that is, of the maximum electron concentration, and the virtual height of the layers obtained by vertical incidence sounding at numerous observatories over a period of many years. The values of the critical frequency and virtual height are derived from examination of ionograms, which though very rich in information, are of difficult interpretation and very expensive in their processing.

It was realized very soon that virtual height may be a misleading parameter in that the time of travel of a radio pulse can be greatly influenced by changes in the distribution of electrons well below the level of reflection as well as by changes in height of the reflection point itself. Consequently, all efforts were focused on critical frequencies studies. The chief result of that epoch can be synthesized by the expression:

$$f_0F2 \propto N_mF2 \propto 1 + 0.02\bar{R}$$

where $\bar{R}$ is the mean Zürich sunspot number, f_0F2 is the critical frequency of the F2 layer and N_mF2, the maximum electron concentration. N_mF2 and f_0F2 values correspond to any midlatitude station, at noontime

(Ratcliffe and Weekes[1960]).

The idea that the above expression could represent the worldwide results has long since been discarded. In fact, at midlatitude stations noon values of N_mF2 are greater in winter than in summer (seasonal anomaly). On the other hand, studies of worldwide f_0F2 data have shown that the anomaly is not exclusively seasonal but contains annual and semiannual components also (Rishbeth[1968]).

With the launching of artificial satellites it was possible to record in ground based stations information about the columnar content of plasma in the ionosphere with excellent temporal resolution and very inexpensive equipment. In recent years the vast amount of observational electron content data, obtained mostly from measurements of the Faraday rotation angle of VHF telemetry transmissions from geostationary satellites, have proven to be a very valuable source of information in studying general aspects of ionospheric physics and transionospheric propagation, (Garriott, da Rosa, and Ross[1970]), and in particular it is an excellent index of the ionospheric response to the solar activity.

Bhonsle, da Rosa, and Garriott[1965], using electron content information from 1958 to 1962 derived from the observation of low orbiting satellites, plotted the noontime values of electron content versus the smoothed sunspot number and observed that the data grouped themselves around three straight lines (see Fig. 1.1) of progressively smaller slopes. The maximum slope corresponded to the straight line connecting all equinoctial points, then followed the slope corresponding to the line connecting the winter points, and finally the smallest slope

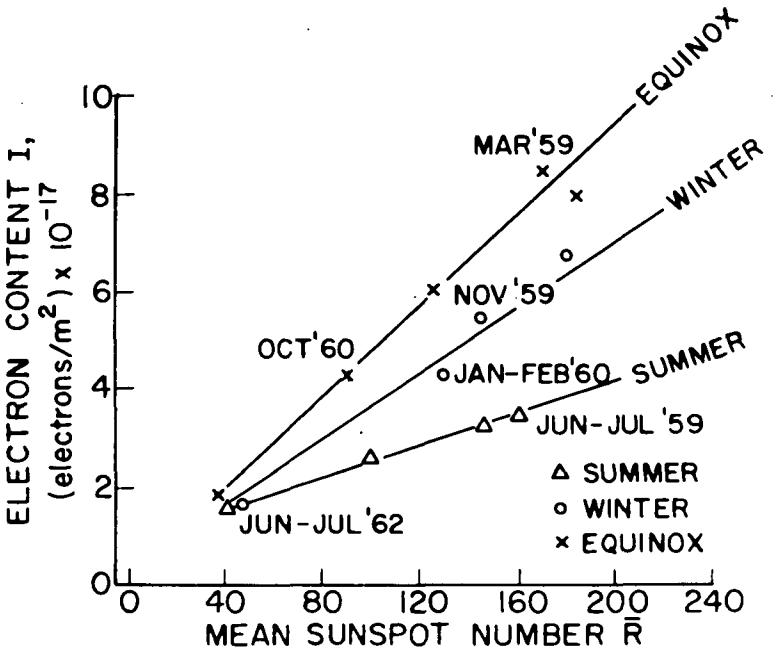

Fig. 1.1. Solar cycle variations of I of midlatitude ionosphere and the mean sunspot number, R. (After Bhonsle, da Rosa and Garriott[1965]).

corresponded to the straight line connecting all summer points. From the graph, they derived the empirical formula:

$$I = [a + b(\bar{R} - 40)] \times 10^{17} \text{ el.m}^{-2} \quad (\text{for } \bar{R} \geq 40)$$

The parameters a and b are constants which are different for different seasons. The data used for these calculations were insufficient to permit a careful study of the seasonal variation of the above relationship and, in view of the relative motion between satellite and observer, these data did not correspond to a fixed ionospheric point. Consequently, all conclusions drawn from that study should be taken with some reser-

vations.

da Rosa et al.[1972] in a preliminary investigation of the influence of the solar activity on the ionospheric electron content used electron content data from 1964 to 1970, obtained from the measurements of the Faraday rotation of VHF telemetry transmissions from ATS (Applications Technology Satellite) and SYNCOM geostationary satellites. In view of the lack of continuous monitoring of EUV radiation, and after an exhaustive cross-correlation analysis between four different solar activity parameters and several ionospheric quantities they adopted for the investigation of long-term effects the half-year mean of the solar radio flux at 2.8 GHz as the index of solar activity and the 31-day mean value of the daily average electron content as the index of electron content.

They concluded that at least over the range of the solar activity represented by the semi-cycle covered, the relationship between electron content and the long-term average of solar microwave flux can be expressed by:

$$\text{IMEAN}_{31} = I_0 + \sigma\langle S\rangle_{183}$$

where σ is defined as the "sensitivity" of the ionosphere to long-term changes in solar activity.

By assuming that long and short term sensitivities are identical it was possible to especialize the above formula to express the prognosticated values of the daily averages of the total electron content

corresponding to observed daily averages of solar radio flux, i.e.:

$$IMEAN_p = I_0 + \sigma S$$

Plots of both $IMEAN_p$ and IMEAN, that is, of the prognosticated and of the observed values of mean daily electron content, showed that the above empirical relation seems to fit reasonably well the data for both low and high solar activity, although, an apparent time-shift between $IMEAN_p$ and IMEAN was observed which suggests that the fluctuations in the real ionosphere lag the corresponding fluctuations of solar flux.

The present work deals with the ionospheric response to fast fluctuations in solar radiation such as those associated with a solar rotation. It is well known that the emission of solar radiation does not occur uniformly over the surface of the sun. Instead, it may be concentrated on certain active areas that can persist for several months, particularly during the years of high solar activity. Consequently, as the sun rotates with a period of about 27 days, solar activity as seen from the earth will seem to vary with that period. The variation in the incident solar radiation is responsible for the appearance of 27-day variations in the earth's ionosphere. In the absence of other effects, the total electron content during one of these 27-day periods will also vary accordingly and so do the rest of ionospheric parameters depending directly upon the photoionization process.

This is basically the idea developed in Chapter 2 where, after showing that the daily averages of the variables involved in the conti-

nuity equation can be expressed in terms of the rotation frequency of the sun only, the continuity equation is solved in the absence of all kinds of drifts except those produced by ambipolar diffusion, to find the time-shift between the daily averages of the solar input and of the total electron content. It is found that the ionospheric delay decreases when solar activity increases. The results found in this chapter do not correspond to the reality because they come from an oversimplified ionospheric model that has resulted from disregarding the action of neutral winds on the electron concentration profile. Nevertheless they are relevant when compared with the results found in Chapter 4, where those drifts were considered, to point out the important role that the neutral winds have in the ionospheric response to the solar input.

In Chapter 3, by using the general feature which describes the behavior of the neutral wind velocities, a feedback mechanism is proposed as part of a non-linear system which simulates the ionosphere. The input to that system is a series of step functions used to approximate a sinusoidal wave of 27-days period representing the daily averages of the solar flux. The response at the output of the system is the electron content. A detailed analysis of the equations involved in the system concludes this chapter.

Chapter 4 has been divided into two parts: the first contains a description of the numerical method used for integrating the set of differential equations involved in the system discussed in Chapter 3, and the last presents the results obtained for periods of time corre-

sponding to the autumnal equinox of low, medium, and high solar activities.

The results found in Chapter 2 show that the sensitivity of the electron content, i.e., the relative variation of the electron content throughout a given period of time, is smaller than the corresponding relative variation of the solar flux, and that the delay of the response electron content to the solar flux decreases when solar activity increases. The conclusion concerning the sensitivity of the electron content is modified later by the results obtained in Chapter 4, when the neutral winds effect on the ionospheric F2 region is included, and the conclusion concerning delay is emphasized.

In Chapter 5, electron content data corresponding to eight different stations and during the period of one year, are statistically analyzed. A creiterion is established in terms of the total signal-to-noise ratio which allows for detecting those periods when the 27-days effect dominates, and the measured delays can be compared with the theoretical ones computed in Chapter 4. When this is done, the agreement is fairly good.

CHAPTER 2

DERIVATION OF THE IONOSPHERIC TIME-RESPONSE TO FLUCTUATIONS IN SOLAR ACTIVITY FROM AN IDEALIZED SOLUTION OF THE CONTINUITY EQUATION

In this chapter the equation of continuity is solved for the electron content to determine the time delay between daily averages of electron content and of the fluctuations of the solar radio flux caused by the 27-day changes in solar radiation.

Let us consider the path between a ground based station placed at a midlatitude point in the northern hemisphere and a geostationary satellite, orbiting at 6.6 Earth radii (see Fig. 2.1). Assuming a linear loss coefficient over the whole path, the continuity equation for electrons is:

$$\frac{\partial N}{\partial t} = q - \beta N - \nabla\cdot(N\vec{V}) \qquad (2.1)$$

where N is the electron concentration

q is the rate of ionization-production

β is the linear loss coefficient

and $\vec{V}$ is the drift velocity due to ambipolar diffusion, neutral winds, and electric fields.

(N, q, β, and $\vec{V}$ are functions of height and time.)

Integrating along the path between the station (observer) and the satellite and calling

$$I \equiv \int_{\text{obs.}}^{\text{sat.}} N\,ds \qquad \text{(Electron content)}$$

$$Q \equiv \int_{obs.}^{sat.} q\,ds \qquad \text{(Integrated production rate)}$$

$$\langle\beta\rangle \equiv \frac{\int_{obs.}^{sat.} \beta N\,ds}{\int_{obs.}^{sat.} N\,ds} \qquad \text{(Weighted mean recombination rate)}$$

Equation 2.1 becomes:

$$\frac{\partial I}{\partial t} = Q - \langle\beta\rangle I - \int_{obs.}^{sat.} [\nabla\cdot(N\vec{V})]\,ds \qquad (2.2)$$

In order to evaluate the relative importance of the integrated transport term (third term on the r.h.s. in Equation 2.2), it is useful to think of the electron content as divided into two parts: the ionospheric content; and the protonospheric part.

To a great extent, the value of the ionospheric electron content is determined by the content of the F2-region, (da Rosa et al. op.cit. [1972]), (a layer consisting mainly of O^+ ions and electrons, the top of which can be placed at roughly 1000 km, where H^+ ions begin to be present in greater concentrations) (Whitten and Poppof[1971]). In this region the ionization is constrained to move along the geomagnetic field lines, except for electromagnetic drifts set up by transverse electric fields important only during storms (Abur-Robb[1969], Amayenc and Vasseur[1972], Bramley and Young[1968], Stubbe and Chandra[1970]).

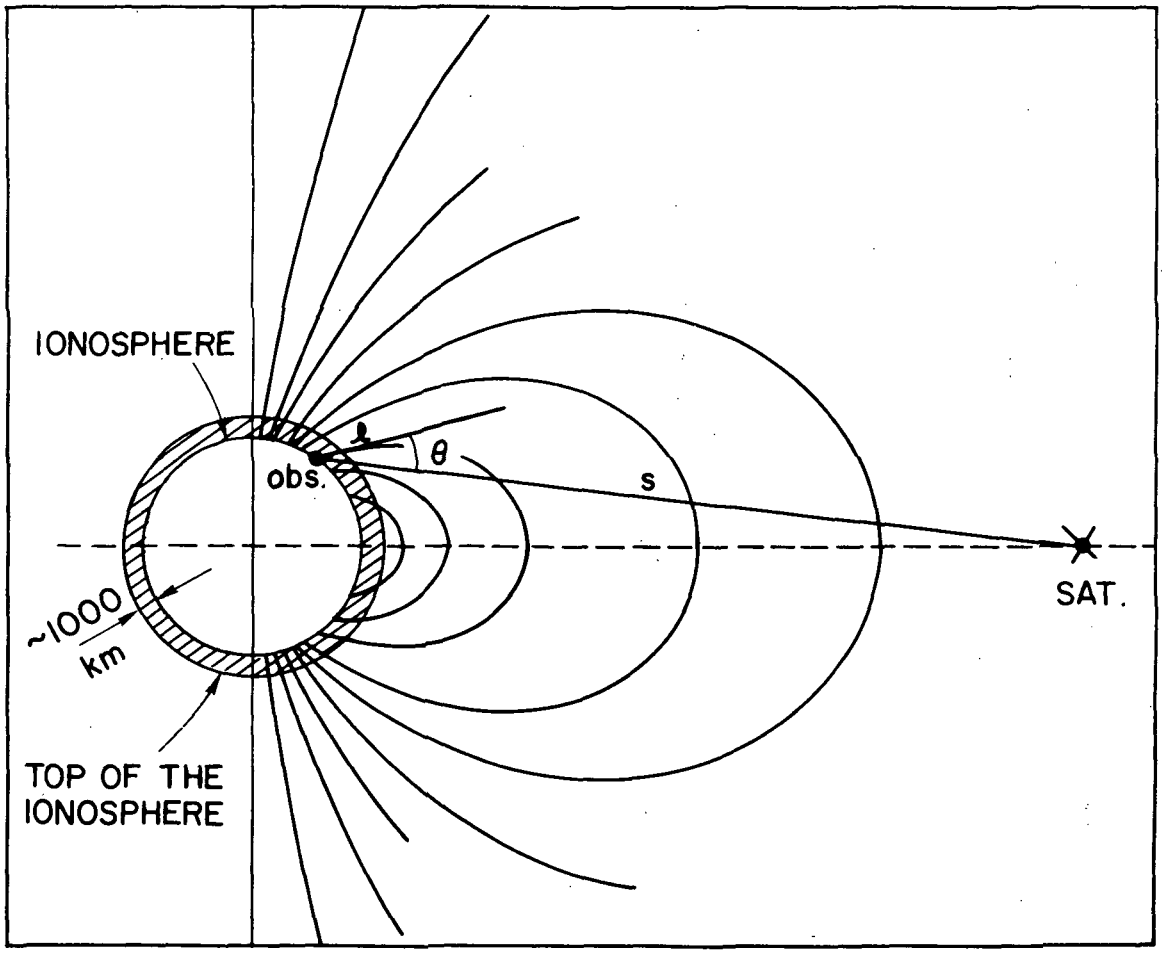

Fig. 2.1. Sketch of a magnetic-meridian cross-section of the earth and its plasma environment, showing that for midlatitude points the lines of force of the earth's magnetic field are practically parallel throughout the ionosphere, which extends to roughly 1000 km.

For midlatitudes, in the ionospheric range of heights, the lines of force of the geomagnetic field are practically parallel, as shown in Fig. 2.1, therefore, the divergence term can be approximated by:

$$\nabla\cdot(N\vec{V}) \approx \frac{\partial}{\partial \ell}(NV_{\ell})$$

where ℓ is measured along the magnetic field line.

If s_i is the value of s at the top of the ionosphere, the integrated transport term can be expressed:

$$\int_o^{s_i} [\nabla\cdot(N\vec{V})]ds \simeq \int_o^{\ell_i} \frac{\partial}{\partial \ell}(NV_\ell)\,\frac{\partial s}{\partial \ell}\,d\ell$$

But $\frac{\partial s}{\partial \ell} = \cos\theta \sim$ constant

where θ is the angle between the magnetic field line and the ray path. Therefore:

$$\int_o^{s_i} [\nabla\cdot(N\vec{V})]ds = \cos\theta \int_o^{\ell_i} \frac{\partial}{\partial \ell}(NV_\ell)\,d\ell = \cos\theta \int_o^{\ell_i} d(NV_\ell) = \Phi_i \cos\theta$$

where Φ_i is the flux along the geomagnetic field line at the top of the ionosphere, i.e. at 1000 km height.

In terms of the topside flux Φ_i, Equation 2.2 becomes:

$$\frac{\partial I}{\partial t} = Q - \langle\beta\rangle I - \Phi_i \cos\theta \qquad (2.3)$$

where all quantities now refer to the ionospheric F2-region.

Whistler observations near L = 4 under quiet conditions have shown a daytime upward flux Φ_i of 3×10^8 el.m^{-2} sec^{-1} and a nighttime downward flux Φ_i of 1.5×10^8 el.m^{-2} sec^{-1} (Park[1970]). Other observations by incoherent scatter radar (Evans[1971], Carpenter and Bowhill[1971]) are in substantial agreement with the whistler results. However, at midlatitudes, still under quiet conditions, whistler observations in-

dicate that the total interchange of flux between the ionosphere and the protonosphere in a 24 hour period is nearly zero (Park, C.G., personal communication). Therefore, if the equation of continuity as given by Equation 2.3 is especialized for daily averages, the last term of the r.h.s vanishes, leaving:

$$\overline{\frac{\partial I}{\partial t}} = \overline{Q} - \overline{\langle \beta \rangle I} \qquad (2.4)$$

On the other hand, when protonospheric content is considered, the transport term cannot be neglected in the continuity equation; in fact, it is the dominant cause of changes in protonospheric content since production and losses are practically nonexistent in that region. However, if daily averages of protonospheric and ionospheric content changes are compared, the former can be disregarded based on the following reason: during daytime the protonospheric content amounts to a small fraction of the total electron content (it has been estimated at about 10% by da Rosa and Garriott[1969], Almeida[1972]). During the night, that fraction becomes important approaching some 50% of the total, but the ratio between daytime and nighttime total electron content generally falls between 5 and 10. Therefore, on a daily average basis the protonospheric content represents a small fraction of the ionospheric content, and the meaning of Equation 2.4 can be extended to represent the general behavior of the quantities between the observer and the satellite.

In Equation 2.3 each of the quantities (which we will represent by the generic symbol x(t)) shows a diurnal variation that will be approximated by a sinusoidal law:

$$x(t) = a_0 + a_1 \cos\omega_E t + a_2 \sin\omega_E t \qquad (2.5)$$

where ω_E is the Earth's rotation frequency, i.e. $\omega_E = 2\pi$ rad.day^{-1}.

In addition, these quantities show a day-to-day change of erratic nature, the cause of which is not yet completely understood. Superimposed on such a random variation there is a systematic response to the fluctuations of solar ionizing energy. These fluctuations are, during periods of high solar activity, associated with discrete active areas in the sun and tend to behave in a sinusoidal fashion with a period of 27 days (the synodical period of the sun's rotation). Since we are investigating the ionospheric response to changes in solar EUV we will treat the erratic day-to-day changes as noise and consider the EUV fluctuations sinusoidal. Thus the coefficients of Equation 2.5 are themselves time-dependent:

$$a_i(t) = a_{i0} + a_{i1} \cos\omega_s t + a_{i2} \sin\omega_s t \quad (i = 0,1,2) \qquad (2.6)$$

where ω_s is the sun's rotation frequency, i.e., $\omega_s = \omega_E/27$.

The functions x(t) are then amplitude modulated sine functions, the modulation being sinusoidal.

Combining Equation 2.6 with 2.5 one obtains:

$$x(t) = X_0 + X_1 \cos\omega_s t + X_2 \sin\omega_s t + X_3 \cos\omega_E t + X_4 \sin\omega_E t$$
$$+ X_5 \cos(\omega_E + \omega_s)t + X_6 \sin(\omega_E + \omega_s)t$$
$$+ X_7 \cos(\omega_E - \omega_s)t + X_8 \sin(\omega_E - \omega_s)t \qquad (2.7)$$

where: $X_0 = a_{00}$ $\qquad$ $X_5 = (a_{11} - a_{22})/2$

$X_1 = a_{01}$ $\qquad$ $X_6 = (a_{21} + a_{12})/2$

$X_2 = a_{02}$ $\qquad$ $X_7 = (a_{11} + a_{22})/2$

$X_3 = a_{10}$ $\qquad$ $X_8 = (a_{21} - a_{12})/2$

$X_4 = a_{20}$

The daily average of x(t) is, by definition:

$$\overline{x(t)} = \frac{1}{T_E} \int_{t-\frac{T_E}{2}}^{t+\frac{T_E}{2}} x(t)dt \qquad (2.8)$$

Substituting the value of x(t), given by Equation (2.7), into the above integral and considering that:

$$\frac{1}{T_E} \int_{t-\frac{T_E}{2}}^{t+\frac{T_E}{2}} \cos\omega_E t \, dt = \frac{1}{T_E} \int_{t-\frac{T_E}{2}}^{t+\frac{T_E}{2}} \sin\omega_E t \, dt = 0 \qquad (2.9)$$

$$\frac{1}{T_E}\int_{t-\frac{T_E}{2}}^{t+\frac{T_E}{2}} \cos\omega_s t \, dt = 0.9977 \cos\omega_s t \qquad (2.10)$$

$$\frac{1}{T_E}\int_{t-\frac{T_E}{2}}^{t+\frac{T_E}{2}} \sin\omega_s t \, dt = 0.9977 \sin\omega_s t \qquad (2.11)$$

$$\frac{1}{T_E}\int_{t-\frac{T_E}{2}}^{t+\frac{T_E}{2}} \cos(\omega_E \pm \omega_s)t \, dt = 0.017 \cos(\omega_E \pm \omega_s)t \qquad (2.12)$$

and

$$\frac{1}{T_E}\int_{t-\frac{T_E}{2}}^{t+\frac{T_E}{2}} \sin(\omega_E \pm \omega_s)t \, dt = 0.017 \sin(\omega_E \pm \omega_s)t \qquad (2.13)$$

It can be seen that in view of the fact that the various coefficients are either near zero or near unity, the daily average of x(t) can be approximated by:

$$\overline{x(t)} = X_0 + X_1 \cos\omega_s t + X_2 \sin\omega_s t \qquad (2.14)$$

Similarly, if we calculate first the time-derivative of both sides of Equation (2.7) and then its daily average, the result can be expressed by the equality:

$$\overline{\frac{\partial x(t)}{\partial t}} = \frac{\partial}{\partial t}\overline{x(t)} \qquad (2.15)$$

Finally, if we consider two functions x(t) and y(t), the diurnal variations of which are given by expressions of the form (2.6), the daily average of the product is:

$$\overline{x(t)y(t)} = \frac{1}{T_E} \int_{t-\frac{T_E}{2}}^{t+\frac{T_E}{2}} (a_0+a_1 \cos\omega_E t + a_2 \sin\omega_E t)(b_0+b_1 \cos\omega_E t + b_2 \sin\omega_E t)dt$$

where all coefficients on the r.h.s. of the equation present a time-dependence of the form given by Equation (2.6). After performing the product indicated under the integral sign, the r.h.s. of the equation is decomposed in a sum of integrals the values of which are given by the expressions labelled from Equation (2.9) to (2.13) from which the nearly-zero coefficients can be disregarded, yielding:

$$\overline{x(t)y(t)} = \overline{x(t)} \times \overline{y(t)} + \frac{1}{2} (a_1 b_1 + a_2 b_2) \qquad (2.16)$$

Applying the results found to the equation of continuity as given by Equation (2.4), one obtains:

$$\frac{\partial}{\partial t} \bar{I} = \bar{Q} - \overline{\langle \beta \rangle} \times \bar{I} - \frac{1}{2} [\langle \beta \rangle_1 i_1 + \langle \beta \rangle_2 i_2] \qquad (2.17)$$

where the term between brackets depends directly on the amplitudes of the diurnal variations of $\langle \beta \rangle$ (weighted recombination rate) and of I (electron content); i.e.:

$$A_I = \left(i_1^2 + i_2^2\right)^{1/2} \qquad \text{(Amplitude of the diurnal variation of I)}$$

$$A_{\langle\beta\rangle} = \left(\langle\beta\rangle_1^2 + \langle\beta\rangle_2^2\right)^{1/2} \qquad \text{(Amplitude of the diurnal variation of } \langle\beta\rangle\text{)}$$

Calling η the ratio between the last two terms on the r.h.s. of (2.17), i.e.:

$$\eta = \frac{\langle\beta\rangle_1 i_1 + \langle\beta\rangle_2 i_2}{2\overline{\langle\beta\rangle} \times \bar{I}} = \frac{1}{2}\left(\frac{A_{\langle\beta\rangle}}{\overline{\langle\beta\rangle}}\right)\left(\frac{A_I}{\bar{I}}\right)\cos\Phi_{\langle\beta\rangle} \qquad (2.18)$$

where $\Phi_{\langle\beta\rangle}$ is the phase difference between the diurnal maximum of $\langle\beta\rangle$ and I, Equation (2.17) takes the form:

$$\frac{1}{\xi}\frac{\partial}{\partial t}\bar{I} + \overline{\langle\beta\rangle} \times \bar{I} = \frac{1}{\xi}\bar{Q} \qquad (2.19)$$

where $\xi = 1 + \eta$

An approximate value of η was obtained using a simulation program of the ionosphere based on the coupled continuity and heat flow equations (Waldman[1971]). The program which makes use of observed values of electron content as one of the necessary boundary conditions, can be operated both in a steady state and in a time-varying mode and its self-consistency is only limited by the fact that the neutral wind is entered as an input, not solved for in a closed form. The diurnal variations of $\langle\beta\rangle$ and I obtained from this program when especialized for a mid-latitude point, a solar radio flux of 175 units and zero wind velocity, are represented in Fig. (2.2). A sinusoidal curve was fitted through the

computed points (dash lines) and from it the ratios below were obtained:

$$\frac{A_{\langle\beta\rangle}}{\beta} = 0.2947$$

$$\frac{A_I}{\bar{I}} = 0.85$$

and $$\cos\Phi_{\langle\beta\rangle} = 0.81$$

Substituting these values into (2.18), a value of 0.10 was found for η.

On the other hand, if (2.19) is written symbolically in the following way:

$$\left(\frac{1}{\bar{\xi}}\frac{\partial}{\partial t} + \overline{\langle\beta\rangle}\right)\bar{I} = \frac{1}{\bar{\xi}}\bar{Q}$$

the first of the two terms between brackets is about three orders of magnitude smaller than the second, since:

$$\frac{1}{\bar{\xi}}\frac{\partial}{\partial t} = \frac{\omega_s}{\bar{\xi}} \sim 10^{-6}\ \text{sec}^{-1}$$

and $$\overline{\langle\beta\rangle} \sim 10^{-3}\ \text{sec}^{-1}$$

therefore Equation (2.19) becomes:

$$\overline{\langle\beta\rangle} \times \bar{I} = \frac{1}{\bar{\xi}}\bar{Q} \qquad (2.20)$$

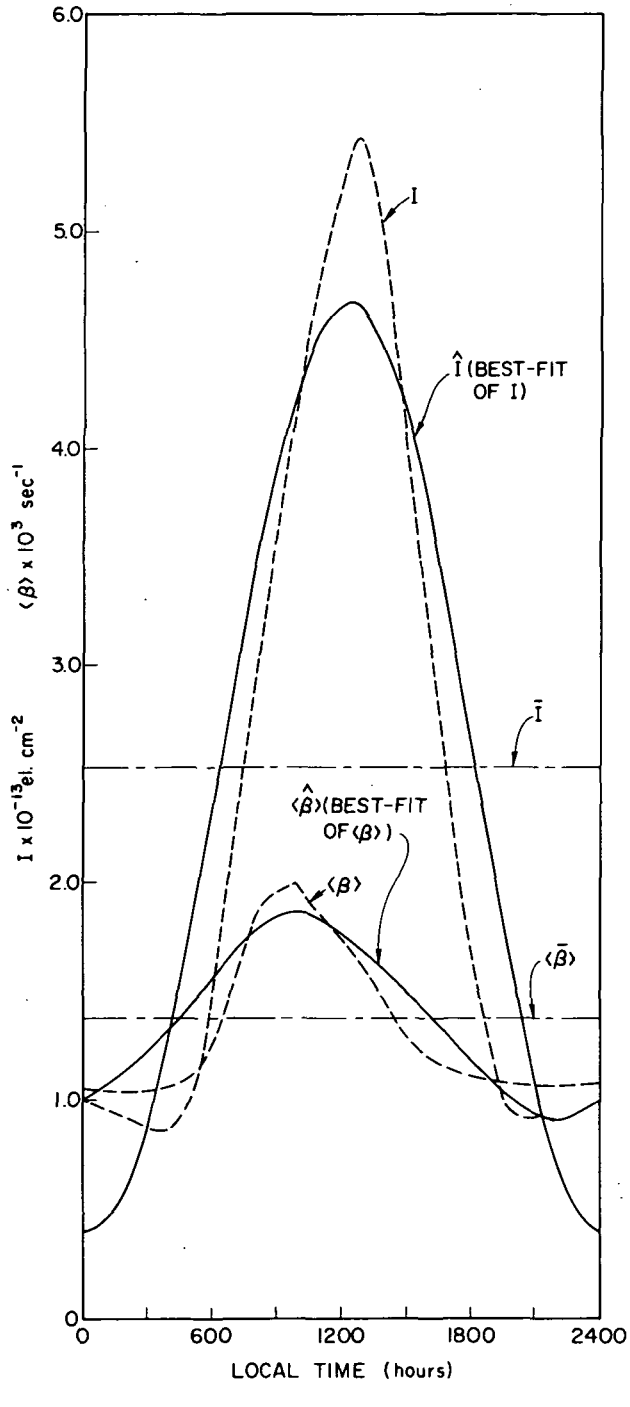

Fig. 2.2. Diurnal variations of $\langle\beta\rangle$ and I, with their corresponding best-fit curves, obtained from a simulation program of the ionosphere based on the coupled continuity and heat flow equations (Waldman[1971]) for the case in which a solar radio flux of 175 units is used.

where $\overline{\langle\beta\rangle}$, $\bar{I}$, and $\bar{Q}$ have the form given by (2.14); i.e.:

$$\overline{\langle\beta\rangle} = \langle\beta\rangle_0 + \langle\beta\rangle_1 \cos\omega_s t + \langle\beta\rangle_2 \sin\omega_s t$$

$$\bar{I} = I_0 + I_1 \cos\omega_s t + I_2 \sin\omega_s t$$

$$\bar{Q} = Q_0 + Q_1 \cos\omega_s t$$

($\bar{Q}$ has been conventionally taken with zero phase).

Substituting the expressions for $\overline{\langle\beta\rangle}$, $\bar{I}$, and $\bar{Q}$ into (2.20), that equation becomes:

$$\left(\langle\beta\rangle_0 + \langle\beta\rangle_1 \cos\omega_w t + \langle\beta\rangle_2 \sin\omega_s t\right)\left(I_0 + I_1\cos\omega_s t + I_2\sin\omega_s t\right) - \frac{1}{\xi}\left(Q_0 + Q_1\cos\omega_s t\right) = 0$$

Since this equation must apply at all values of time, the coefficients of $\cos\omega_s t$, $\sin\omega_s t$, and the time independent part must, separately, be equal to zero. Therefore the above equation is separated into three equations independent of time from which the following expression for the delay-time between $\bar{I}$ and $\bar{Q}$ is obtained:

$$\delta_I = \frac{1}{\omega_s} \arctan \frac{\left(1 - \frac{1}{2} D_{\langle\beta\rangle} D_Q \cos\omega_s \delta_{\langle\beta\rangle}\right)\sin\omega_s \delta_{\langle\beta\rangle}}{\frac{D_Q}{D_{\langle\beta\rangle}} + \frac{1}{2} D_{\langle\beta\rangle} D_Q \sin^2\omega_s \delta_{\langle\beta\rangle} - \cos\omega_s \delta_{\langle\beta\rangle}} \qquad (2.21)$$

where $D_Q = \dfrac{Q_1}{Q_0}$ (Ratio between the amplitude of the a.c. term and the mean, for production)

$D_{\langle\beta\rangle} = \dfrac{\sqrt{\langle\beta\rangle_1^2 + \langle\beta\rangle_2^2}}{\langle\beta\rangle_0}$ (Ratio between the amplitude of the a.c. term and the mean, for recombination)

$$\tan\omega_w\delta_{\langle\beta\rangle} = \frac{\langle\beta\rangle_2}{\langle\beta\rangle_1}$$ (Phase of the recombination rate with respect phase of the production term)

and $$\tan\omega_s\delta_I = \frac{I_2}{I_1}$$ (Phase of the electron content with respect phase of the production term)

The unknowns on the r.h.s. of Equation (2.21) are $D_{\langle\beta\rangle}$ and $\delta_{\langle\beta\rangle}$, the determination of which in terms of the solar input can be carried out in the following way:

By definition, the daily average of the weighted mean of the recombination coefficient is:

$$\overline{\langle\beta\rangle} = \overline{\left(\frac{\int_{h_o}^{h}\beta N\,dh}{\int_{h_o}^{h}N\,dh}\right)} = \frac{1}{m}\left[\sum_{i=1}^{m}\frac{\int_{h_o}^{h}\beta_i N_i\,dh}{\int_{h_o}^{h}N_i\,dh}\right]\sec^{-1} \qquad (2.22)$$

where m is the number of $\langle\beta\rangle$ values over which the mean is taken,

β is the linear loss coefficient (function of height and time),

N is the electron concentration (function of height and time),

h_o is the lower boundary of the F2-region,

and h is the independent variable height.

In order to determine the r.h.s. of Equation (2.22) it is necessary to know the neutral composition of the atmosphere, since β is a linear combination of the neutral concentrations of N_2 and O_2, and the electron concentration profile.

For each individual gas in the atmosphere, the variation of its concentration with height is given by the barometric law; i.e.:

$$n(h) = n(h_o) \times \frac{T(h_o)}{T(h)} \exp\left[- \int_{h_o}^{h} \frac{dh}{H(h)} \right] \text{ cm}^{-3} \qquad (2.23)$$

where $n(h)$ and $n(h_o)$ are the concentrations at heights h and h_o, respectively; $T(h)$ and $T(h_o)$ are the corresponding neutral temperatures in °K and $H(h)$ is the scale height.

The vertical distribution of temperature, $T(h)$, can be expressed in terms of the exospheric temperature using the empirical formula (Bates[1959], Jacchia[1965]):

$$T(h) = T_\infty - (T_\infty - T_o) \exp[- \alpha(h - h_o)] \ ^\circ K \qquad (2.24)$$

where $T_o = T(h_o)$, T_∞ is the exospheric temperature, h and h_o are expressed in kilometers and α is a parameter with dimensions km^{-1}, different for each profile, the value of which is:

$$\alpha = 0.0291 \exp\left(- \frac{\xi^2}{2}\right)$$

where $$\xi = \frac{T_\infty - 800}{750 + 1.722 \times 10^{-4}(T_\infty - 800)^2} \qquad \text{(with } T_\infty \text{ in °K)}$$

On the other hand, the exospheric temperature can be expressed in terms of only the solar input and local time using the formula, (Nisbet[1971]):

$$T_\infty = \sum_{j=0}^{5} C_j \cos\left(\frac{2\pi jHL}{24}\right) + \sum_{j=1}^{5} S_j \sin\left(\frac{2\pi jHL}{24}\right) \qquad (2.25)$$

where C_j and S_j are coefficients given in terms of the daily average of the 10.7 cm solar flux, and HL is the local time.

The validity of the empirical formula (2.24), which gives the neutral temperature profile, was checked by especializing (2.25) for HL = 12 and for three different levels of solar activity (daily averages of solar flux considered were $\overline{S}$ = 75 units, $\overline{S}$ = 150 units, and $\overline{S}$ = 250 units). With the three exospheric temperatures obtained and T_o = 355 °K it was possible to draw the corresponding profiles. Fig. (2.3) represents the profiles obtained with the empirical formula (dashed lines) and those derived from the standard model CIRA[1965] (continuous lines) which gives all atmospheric quantities in tabular form. It can be seen that the agreement between every pair of curves is quite good in the high solar activity case and acceptable in the other two.

Substituting Equation (2.24) into (2.23) this Equation can then be written:

$$n(h) = \frac{n(h_o) \times T(h_o)}{T_\infty - (T_\infty - T_o)\exp[-\alpha(h-h_o)]} \exp\left[-\frac{m}{k} \int_{h_o}^{h} \frac{g(h)\, dh}{T_\infty - (T_\infty - T_o)\exp[-\alpha(h-h_o)]} \right] \qquad (2.26)$$

where $H(h) = \frac{kT(h)}{mg(h)}$

Calling R_E the radius of Earth, then the geopotential height above the lower boundary of the F2 region is, by definition:

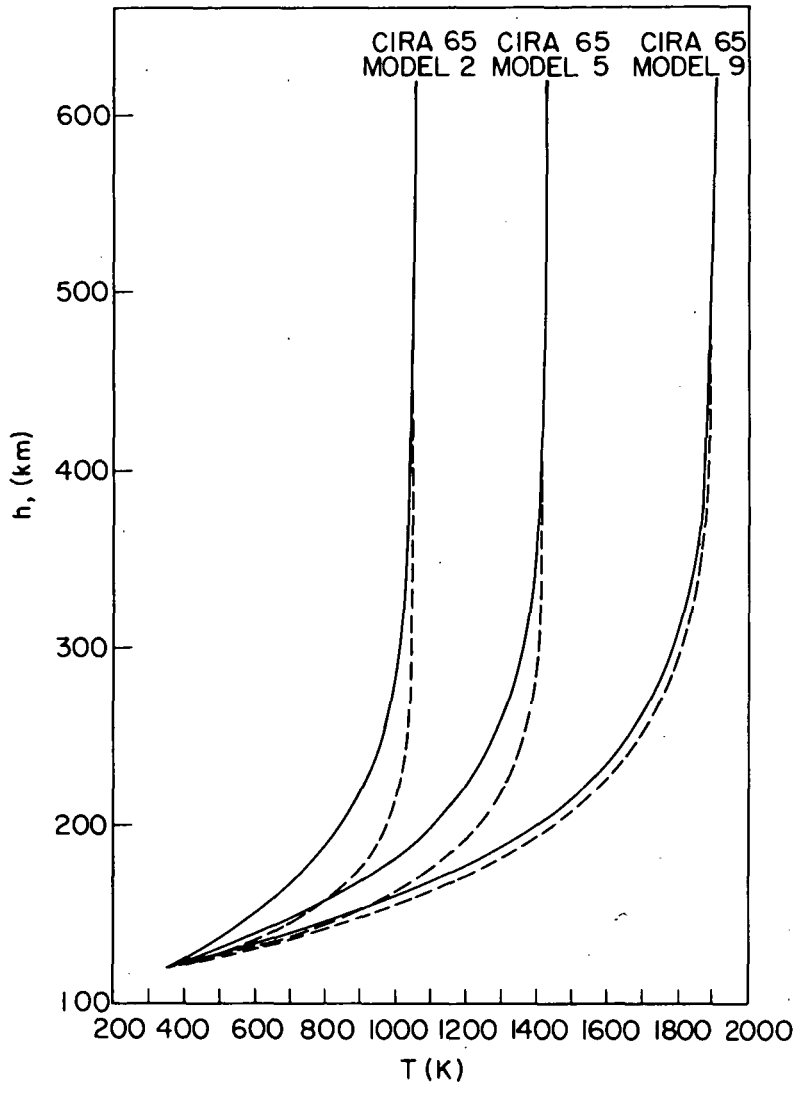

Fig. 2.3. Vertical distribution of temperature at noon for low solar activity (S = 75 units), medium solar activity (S = 150 units), and high solar activity (S = 250 units). Dashed lines: The profile was obtained by using the empirical formula given by Bates[1959], Jacchia [1965]. Continuous lines: The profile was derived from the standard model CIRA[1965] which gives all atmospheric quantities in tabular form.

$$h^* \equiv \int_{h_o}^{h} \left(\frac{R_E}{R_E + h} \right)^2 dh = R_E \left(\frac{h - h_o}{R_E + h} \right)$$

Assuming further, that:

$$g(h) = g(h_o)$$

the integral term of (2.26) can be easily solved and the neutral concentration will be given in terms of only the solar input, local time, and height; i.e.:

$$n(h^*) = n_o F^{-p} \exp(\alpha h^*) \qquad (2.27)$$

where $F = \dfrac{T_\infty \exp(\alpha h^*) - (T_\infty - T_o)}{T_o}$

and $p = 1 + \dfrac{1}{\alpha H_\infty}$

with $H_\infty = \dfrac{kT_\infty}{mg_o}$, the exospheric scale height.

The linear loss coefficient, β, is given by the formula:

$$\beta = \gamma_{N_2} [N_2] + \gamma_{O_2} [O_2] \quad \sec^{-1} \qquad (2.28)$$

where, according to Hintereger et al.[1965],

$$\gamma_{N_2} = 2 \times 10^{-12} \text{ cm}^3 - \text{sec}^{-1}$$

$$\gamma_{O_2} = 3 \times 10^{-11} \text{ cm}^3 - \text{sec}^{-1}$$

and the N_2 and O_2 concentrations, namely $[N_2]$ and $[O_2]$ in Equation (2.28), are obtained from (2.27).

The electron concentration profile was derived assuming diffusive equilibrium in the ionosphere; i.e.:

$$\nabla \cdot (N\vec{v}) = 0$$

Ignoring the action of horizontal pressure gradients, drifts caused by electric fields and assuming that the vertical gradients of $N\vec{v}$ greatly exceed the horizontal gradients, the above equation takes the form:

$$\frac{\partial}{\partial h} (NW_D) = 0 \qquad (2.29)$$

where W_D is the vertical diffusion velocity, given by:

$$W_D = -D_p \left(\frac{1}{2H} + \frac{1}{N} \frac{\partial N}{\partial h} \right)$$

The diffusion coefficient, D_p, increases exponentially upwards and may be written as:

$$D_p = D_o \, e^{\frac{h-h_o}{H}}$$

Substituting D_p and W_D into (2.29) and performing the operation indicated by the derivative sign, that equation becomes the classical one derived by Ferraro in 1945:

$$\frac{d^2N}{dh^2} + \frac{3}{2H}\frac{dN}{dh} + \frac{N}{2H^2} = 0$$

The general solution of this differential equation, for the case of H independent of height, is:

$$N(h) = A \exp[(h - h_o)/H] + B \exp[(h - h_o)/2H]$$

The two boundary conditions imposed to this solution, in order to determine the integration constants A and B, are:

$$\text{At } h = h_o \qquad N(h_o) = 0$$

$$\text{At } h = h_{max} \qquad N(h_{max}) = N_{max}$$

where h_{max} is the height of the peak of the F2 layer.

After expressing the two integration constants in terms of the boundary conditions, the electron concentration is given by:

$$N(h) = N_{max} \frac{\exp[-(h - h_{max})/2H] - \exp[-(2h - h_o - h_{max})/2H]}{1 - \exp[-(h_{max} - h_o)/2H]} \qquad (2.30)$$

The height of the peak, h_{max}, is determined at any time of the day by the criterion given by Rishbeth and Barron[1960]; i.e. the height of the peak under diffusive equilibrium conditions occurs where:

$$\frac{\beta}{d} = 0.6 \quad \text{(During daytime)}$$

and where

$$\frac{\beta}{d} = 0.13 \quad \text{(During the night)}$$

d is the so-called diffusion rate and is given by:

$$d = \frac{D_p \sin^2 \Psi}{H^2} \sec^{-1}$$

where D_p, the plasma diffusion coefficient, is given in terms of the neutral temperature in °K, and composition in cm^{-3} by the empirical formula:

$$D_p = 1.2 \times 10^{17} T^{0.7} / \left([O] + [N_2] \right) \ cm^2 \times sec^{-1}$$

Ψ is the dip angle and H the scale height. Therefore, h_{max}, and consequently the electron concentration as given by (2.30) is expressed in terms of the solar input and local time.

Substituting (2.28) and (2.30) into (2.22) this equation can now be expressed in terms of only the solar input. A computer program was prepared to find the corresponding daily values of $\overline{\langle \beta \rangle}$ for an assumed solar input, such as:

$$\bar{S} = S_o + S_1 \cos\omega_s t \qquad (2.31)$$

The daily average of the integrated production rate was assumed to be proportional to the daily average of the solar flux and therefore:

$$\bar{Q} = Q_o + Q_1 \cos\omega_s t$$

By taking in all calculations realistic values of S_o and S_1; i.e. of D_Q, a set of 32 consecutive values of $\bar{S}$ was obtained from (2.31) for three different levels of solar activitv.

We note that the expression given by Nisbet for the diurnal variation of the exospheric temperature in terms of local time and daily average of the solar radio flux does not include any phase information. However, it has been established that there is a systematic one day delay in the response of neutral temperature to changes in the solar radio flux (Bourdeau, Chandra, and Neupert[1964], Chandra and Krishnamurthy[1967], Thomas and Ching[1969], Herman and Chandra[1969]). Consequently, we want to introduce back delay in the Nisbet formula. If we consider again the expression of the exospheric temperature:

$$T_\infty = \sum_{j=0}^{5} C_j \cos\left(\frac{2\pi jHL}{24}\right) + \sum_{j=1}^{5} S_j \sin\left(\frac{2\pi jHL}{24}\right)$$

its daily average will be:

$$\bar{T}_\infty = C_o(\bar{S})$$

and taking account of the 1 day delay between $\overline{T}_\infty$ and $\overline{S}$, this expression can be written, after considering (2.31):

$$\overline{T}_\infty = C_o[\overline{S}(t - 1)] \quad \text{(with t in days)}$$

The diurnal variation of the exospheric temperature can then be written:

$$T_\infty = \overline{T}_\infty + \sum_{j=1}^{5} \left[C_j \cos\left(\frac{2\pi jHL}{24}\right) + S_j \sin\left(\frac{2\pi jHL}{24}\right)\right] \qquad (2.32)$$

Every consecutive value of $\overline{S}$ was substituted into (2.22) from which the corresponding daily average of the weighted mean recombination coefficient, $\overline{\langle\beta\rangle}$ was determined. The result was a set of 32 values of $\overline{\langle\beta\rangle}$ which were passed through a mathematical best-fit filter from which $D_{\langle\beta\rangle}$, and $\delta_{\langle\beta\rangle}$ were obtained.

With the purpose of finding realistic values for the coefficients of Equation (2.31) under low solar activity conditions, a plot was made of the solar radio flux at 2.8 GHz for the period of 6 May 1965 through 1 June 1965. (Fig. 2.4) The choice of this particular period of time was dictated by the quasi-sinusoidal character of the solar flux, i.e. by the absence of strong erratic changes, which, in the context of the present work, are considered as noise. Daily average values of the radio flux were plotted together with the corresponding best-fit sinusoidal curve from which the following values were derived:

$$S_0 = 81 \text{ units}$$

$$S_1 = 12 \text{ units}$$

and therefore:

$$D_S = \frac{S_1}{S_0} = 0.15$$

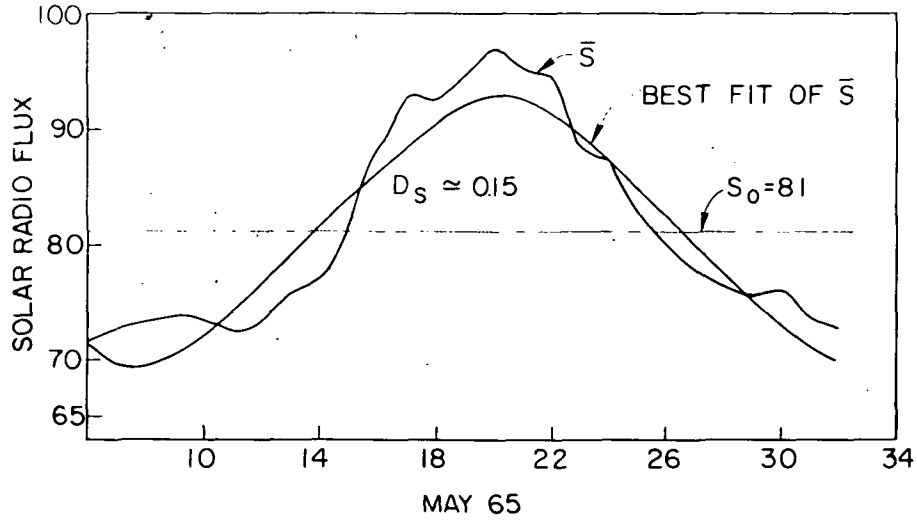

Fig. 2.4. Graph of the solar radio flux at 2.8 GHz for the period of 6 May 1965 through 1 June 1965, and its best-fit curve from which the long term average, S_0, and amplitude, S_1, were derived.

Fig. (2.5, Curve a) represents the variation of the daily average of the integrated production rate. This curve, drawn conventionally with zero phase, was derived using the previously mentioned assumption of considering the daily average of the integrated production rate to be proportional to the daily average of solar flux, that is:

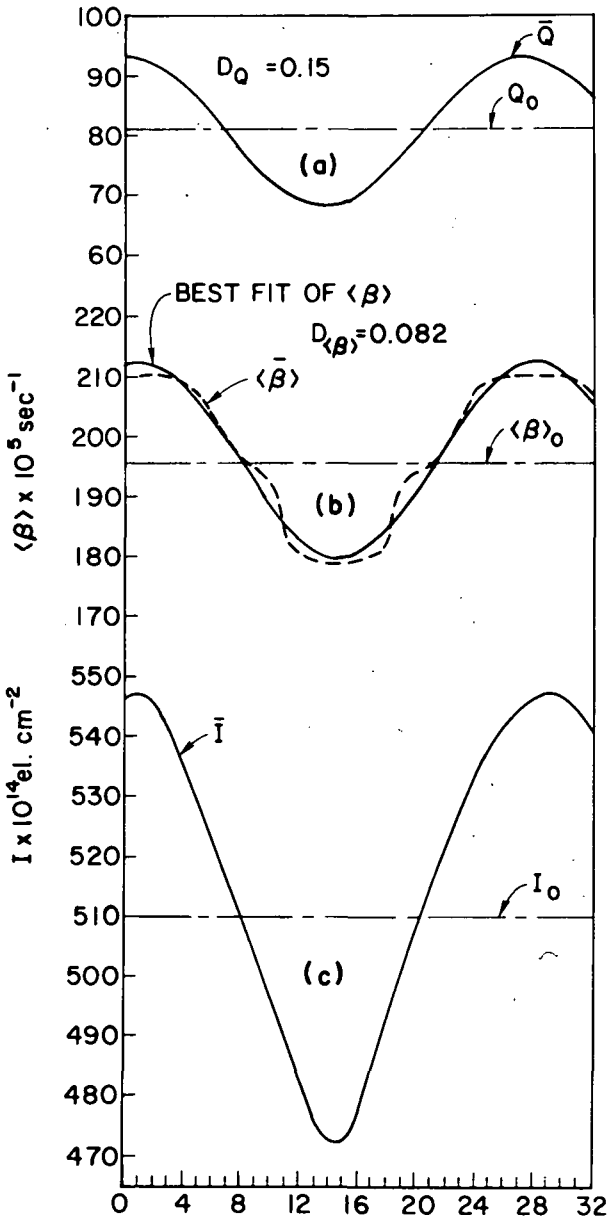

Fig. 2.5. Curve (a). Assumed variation of the daily average of the integrated production rate.

Fig. 2.5. Curve (b). Variation of the daily average of $\langle\beta\rangle$ throughout 32 consecutive days and the corresponding best-fit curve.

Fig. 2.5. Curve (c). Theoretical variation of the daily average of the electron content, derived by assuming a $Q_o = 10^{12} cm^{-2}$, throughout 32 consecutive days.

$$D_Q = D_S = 0.15$$

Curve (2.5b) represents the daily average of $\langle\beta\rangle$, the weighted mean of the recombination coefficient, and its best-fit from which it was found that:

$$D_{\langle\beta\rangle} = 0.082$$

Since a one day delay between S and the atmospheric temperature was assumed:

$$\delta_{\langle\beta\rangle} \sim 1 \text{ day}$$

Curve (2.5c) was drawn by assuming a $Q_o = 10^{12}$ el.cm^{-2}, which is a reasonable value of the integrated production rate for the level of solar activity considered. By substituting the values of D_Q, $D_{\langle\beta\rangle}$, and $\delta_{\langle\beta\rangle}$ found in Equation (2.21) the delay of the electron content with respect to the solar input was determined. The result is:

$$\delta_I = 1.15 \text{ days}$$

In addition, since δ_I has been derived from an equation of the form:

$$\overline{\langle\beta\rangle} \times \overline{I} = \overline{Q}$$

the sensitivity of the electron content, that is $\frac{\Delta\bar{I}}{\bar{I}}$, will be given by:

$$\frac{\Delta\bar{I}}{\bar{I}} = \frac{\Delta\bar{Q}}{\bar{Q}} - \frac{\Delta\overline{\langle\beta\rangle}}{\overline{\langle\beta\rangle}}$$

or:

$$D_I = D_Q - D_{\langle\beta\rangle} \qquad (2.33)$$

which gives, in this case:

$$D_I = 0.068$$

The same procedure was applied to a set of values of solar flux covering the whole range of solar activity, (from S_0 = 80 units to S_0 = 280 units). In order to facilitate comparison, identical values of D_Q were used for all solar activity levels. The results are synthesized in Table 1.

From the observation of this table the following conclusions can be drawn:

a) The delay of the electron content decreases when solar activity increases. Using the information given in the first and third columns, a plot of the delay δ_I versus the solar flux averaged over several solar rotations, S_0, was made (Fig. (2.6)). A best-fit exponential curve was passed through all δ_I vs. S_0 points which allows for writing the following relationship:

$$\delta_I = 3.6 \exp(-0.012 \times S_0) \text{ days} \qquad (2.34)$$

TABLE 1

$D_Q = 0.15 \qquad \delta_\beta = 1$ day

S_0	D_β	δ_I (days)	D_I
80	0.085	1.2	0.065
100	0.077	0.990	0.073
120	0.0705	0.836	0.080
140	0.0671	0.767	0.083
160	0.0541	0.570	0.096
180	0.0536	0.550	0.0964
200	0.0502	0.490	0.0998
220	0.0345	0.288	0.115
240	0.025	0.197	0.125
260	0.0189	0.145	0.1311
280	0.0148	0.1	0.135

The preceding equation, although representing an empirical fit of calculated points, is more convenient than (2.21), not only because it is simpler, but also because it expresses δ_I in terms of the averaged solar flux over several solar rotations only. It should be noted that Equation (2.34) is applicable also to cases in which different values of D_Q are used.

b) The sensitivity of the electron content is smaller than the sensitivity of the integrated production rate and increases with solar activity. This is caused by the fact that $D_{\langle\beta\rangle}$ in Equation (2.33) has the same sign as does D_Q (i.e. the recombination coefficient $\overline{\langle\beta\rangle}$ increases when solar radiation increases) and therefore:

$$D_I < D_Q$$

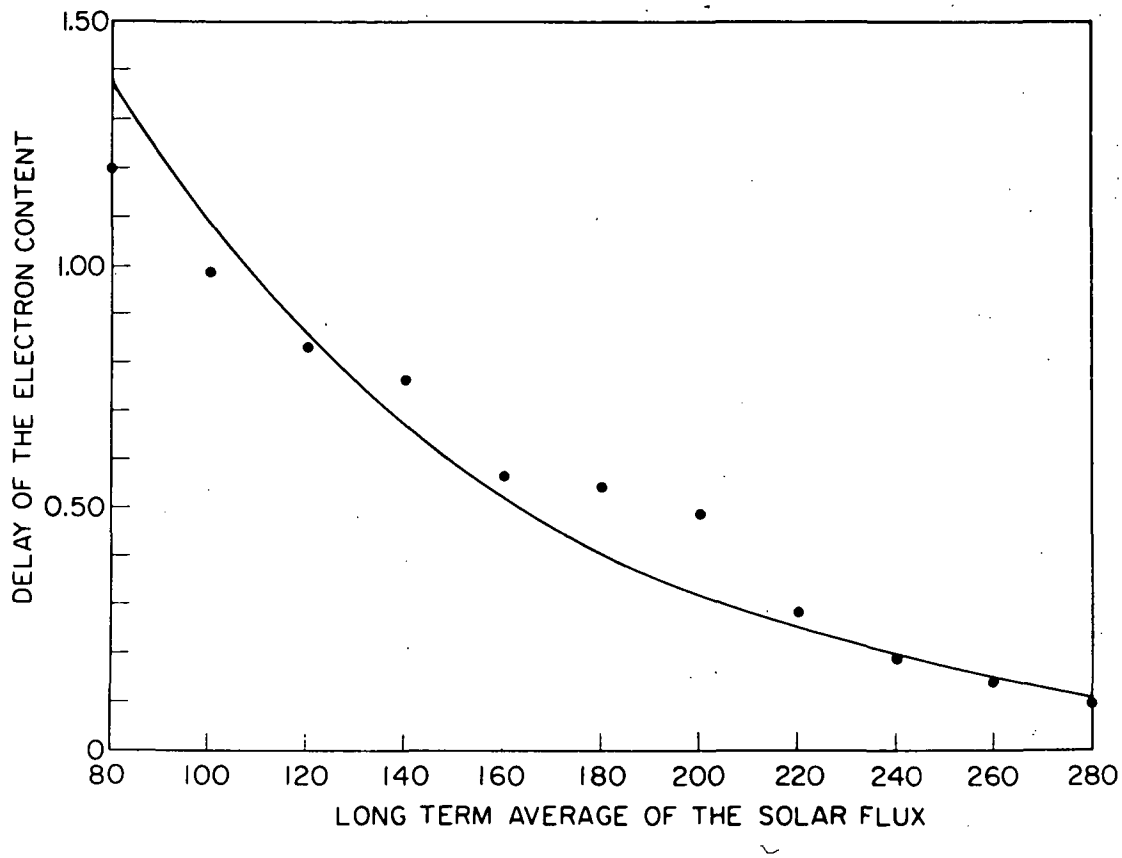

Fig. 2.6. Scatter diagram of electron content delay versus long term average of the solar flux, and the best-fit curve through the scattered points.

Thus the variations in $\overline{\langle\beta\rangle}$ moderate the changes in $\bar{I}$ due to varying solar inputs.

The fact that the daily average of the recombination coefficient increases with solar radiation can be understood in the following way: When solar activity increases the concentration of N_2 increases at all levels, producing an increase in β, the linear loss coefficient. However, the height of the peak does not vary substantially. As a matter of fact, it was found, after applying the Rishbeth criterion to determine the height of the peak to CIRA models 2 and 3, that a variation of 25% in solar flux produces a variation in the height of the peak of only 6.4%. Since the weighting factor in the expression of $\overline{\langle\beta\rangle}$, i.e., the electron concentration, increases in the same amount in the numerator and in the denominator does not affect the value of this parameter because the height of the peak is practically constant and therefore $\overline{\langle\beta\rangle}$ will increase as a consequency of the increase in β.

As shown in Chapter 5 where experimental observations are examined, frequently conclusion (b) is violated, i.e., frequently the relative variation in electron content is larger than the relative variation in solar flux. This brings out one of the limitations of the simple model developed in this Chapter. In Chapters 3 and 4 we introduce the effect of neutral winds on the ionization and find that the sensitivities of electron content can become larger than those of the solar flux.

CHAPTER 3

THE NEUTRAL WIND FEEDBACK MECHANISM

In the preceding chapter the ionospheric response to the 27-day solar ionizing radiation was determined for the hypothetical case in which the action of neutral winds was disregarded.

The general effect of the neutral wind on the ionospheric F2-layer (as discussed by King and Kohl[1965]) is to move the ionization along the magnetic field lines. During daytime the meridional wind blows poleward and tends to push the ionization down, while during the night, the meridional wind blows equatorward and tends to lift the ionization. The effect of the downward drift, during the day, is to move the F2-layer into a region of larger loss rate and thus to decrease the electron concentration and the columnar electron content, the reverse taking place at night.

The above effect of the neutral winds is considered in this chapter in an investigation of the interaction between the 27-day solar ionizing radiation and the electron content. An analytical study of the dynamic properties of the upper atmosphere is complicated by the need of solving a large number of coupled differential equations (Stubbe[1970]). In the F-region range of heights the neutral air is a mixture of mainly diatomic nitrogen and monoatomic oxygen while the ionosphere contains electrons and monoatomic oxygen ions. For each of these particle species one has to solve a continuity equation, three components of the equation of motion, and the heat-transfer equation. In other words, a set of twenty coupled differential equations must be dealt with.

The large amount of computer time that would be required to solve these equations, the mathematical acrobatics associated with the stability of the solution, and finally the uncertainties in the determination of the boundary conditions that must be imposed on the problem, suggest a "non-standard" procedure to solve this particular problem, one which will make use of all possible simplifications without compromising the result.

Since the output to the procedure must be the daily averages of the electron content throughout the period considered, the main simplification consists of choosing from among the instantaneous values of the diurnal variation of the electron content, one that can be used as an index of the daily average.

With that purpose, a study was made of the cross-correlation coefficient between values of the electron content taken every 30 minutes and the corresponding daily average. The data used correspond to the Stanford ATS-1 station, where the system used for recording electron content data takes one sample every five minutes or 288 samples per day. The period chosen was the whole year of 1969. It was found that the electron content measured at any hour during daytime correlates fairly well with the corresponding daily average (correlation coefficient $\rho \geq 0.7$). In particular the electron content measured near the middle of the day presented a correlation coefficient of the order of 0.9 when compared with daily averages. We chose to work with the content observed near 1400 L.T. because at that time the continuity equation can be solved for the homogeneous case, that is, the ionosphere can be considered

under steady-state conditions.

Let us now consider a steady-state ionosphere at 1400 L.T. subjected to a certain ionizing flux. To reduce the number of equations to be considered, a model for the neutral atmosphere can be adopted. Values of the electron concentration N(h) and of neutral wind velocities $V_n(h)$ as well as the resulting electron content can be computed in a self-consistent way. If now the ionizing radiation is allowed to suffer a step increase the following chain of events is triggered: production and consequently ionization goes up immediately. This causes an increase in ion-drag and a reduction in wind velocity. Since the midday wind is poleward, as stated above, and forces the ionization into lower heights, a reduction in this wind will allow the plasma to rise causing the average recombination coefficient to become smaller. This, in turn, allows the electron concentration to increase further and reduces the wind velocity even more. There is, therefore, under these conditions, a positive feedback in the ionosphere which produces a relative increase in electron content larger than the relative increase in ionizing radiation. After a certain delay, generally accepted to be of about 1 day as pointed out in the preceding chapter, the augmented energy input to the higher atmosphere will result in a neutral temperature elevation which causes a decrease in the pressure gradient forces that drive the winds, and consequently, a new reduction in the wind velocity. Therefore, the electron concentration will increase even further, increasing the ion-drag force so that the wind velocity will again decrease.

When one considers the positive feedback described above, one is

confronted with the question of why the system does not run away. An idea of the mechanism that limits the increase in electron content can be obtained by considering a much simplified model in which diffusion is neglected and losses are simply equated to production. Although patently unrealistic, such a model allows one to visualize the limitation mechanism. One can, under such circumstances, write:

$$q_{max} = \beta_{max} \times N_{max} \qquad (3.1)$$

where the subscript serves to indicate the fact that the equation is to be applied to quantities at the height of maximum ionization.

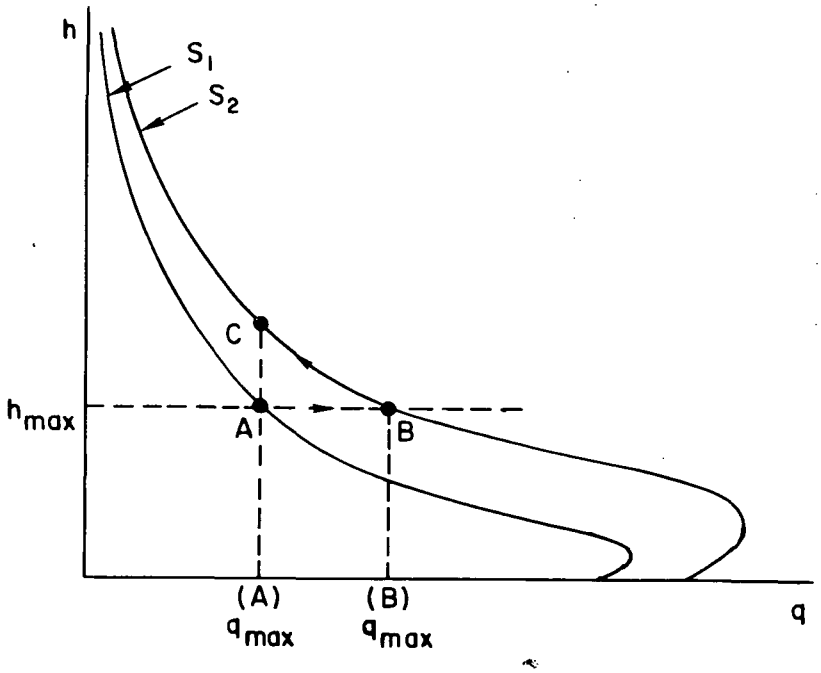

Fig. 3.1. Production rate profiles, corresponding to two different levels of solar radiation, S_1 and S_2, used in the text to visualize the limiting mechanism of the increase in electron content when the solar radiation changes suddenly from S_1 to S_2.

Let us now inquire what happens when the solar radiation changes abruptly from a value S_1 to a larger value S_2. Figure (3.1) represents two possible production rate profiles corresponding to these two levels of radiation. Under S_1 solar activity conditions the height of the peak occurs at the point A, where according to (3.1):

$$q_{max}^{(A} = \beta_{max}^{(A} \times N_{max}^{(A}$$

If now the solar activity suddenly changes to the S_2 value, production and ionization will change instantly in such a way that the new situation will be represented by the point B where:

$$q_{max}^{(B} = \beta_{max}^{(B} \times N_{max}^{(B} \qquad (3.2)$$

in which $\beta_{max}^{(B} = \beta_{max}^{(A}$.

If neutral winds are not considered, Equation (3.2) will represent the new equilibrium situation. If the neutral wind effect is taken into account the variation in N_{max} will cause a variation in neutral winds velocity which in turn will lead to a variation in the height of the peak. Therefore, the point B of Figure (3.1) will move up along the curve corresponding to the solar radiation S_2.

At any h_{max} corresponding to the range of variation of q_{max} in the interval BC, the production rate is such that:

$$q_{max}^{(A} \leq q_{max} = q_{max}^{(B} \exp -\left(\frac{\Delta h_{max}}{H}\right)$$

Therefore:

$$\Delta h_{max} \leq H \times \ln\left[\frac{q_{max}^{(B}}{q_{max}^{(A}}\right] \qquad (3.3)$$

Expression (3.3) indicates that the height increase will stop before h_{max} reaches the value corresponding to the point C, i.e., the new equilibrium will occur when the layer has risen to such a height that the new q_{max} is slightly larger than the q_{max} prior to the increase in radiation.

The stability of the system can be demonstrated in a more convincing manner through the use of the computer program described in detail in Chapter 4. This program models the reaction of the ionosphere to sudden changes in ionizing radiation by solving the continuity equation under the action of a given neutral wind and then computing the wind velocity consistent with the calculated ionization. The new wind information is used to recompute the ionization, from which a correction to the wind velocity is obtained. The iterations are carried out until a stable, self-consistent solution is obtained. The program, in fact, produces a sequence of solutions that carry q_{max} along the q-profile from B to C', the new equilibrium point.

Figures (3.2a) through (3.2c) show three typical situations. These curves are plots of production rates versus height for low, medium, and high solar activity. Point A represents the production rate at the height of the peak under S_1 solar activity conditions, while point C represents the limiting situation predicted by Equation (3.3). In

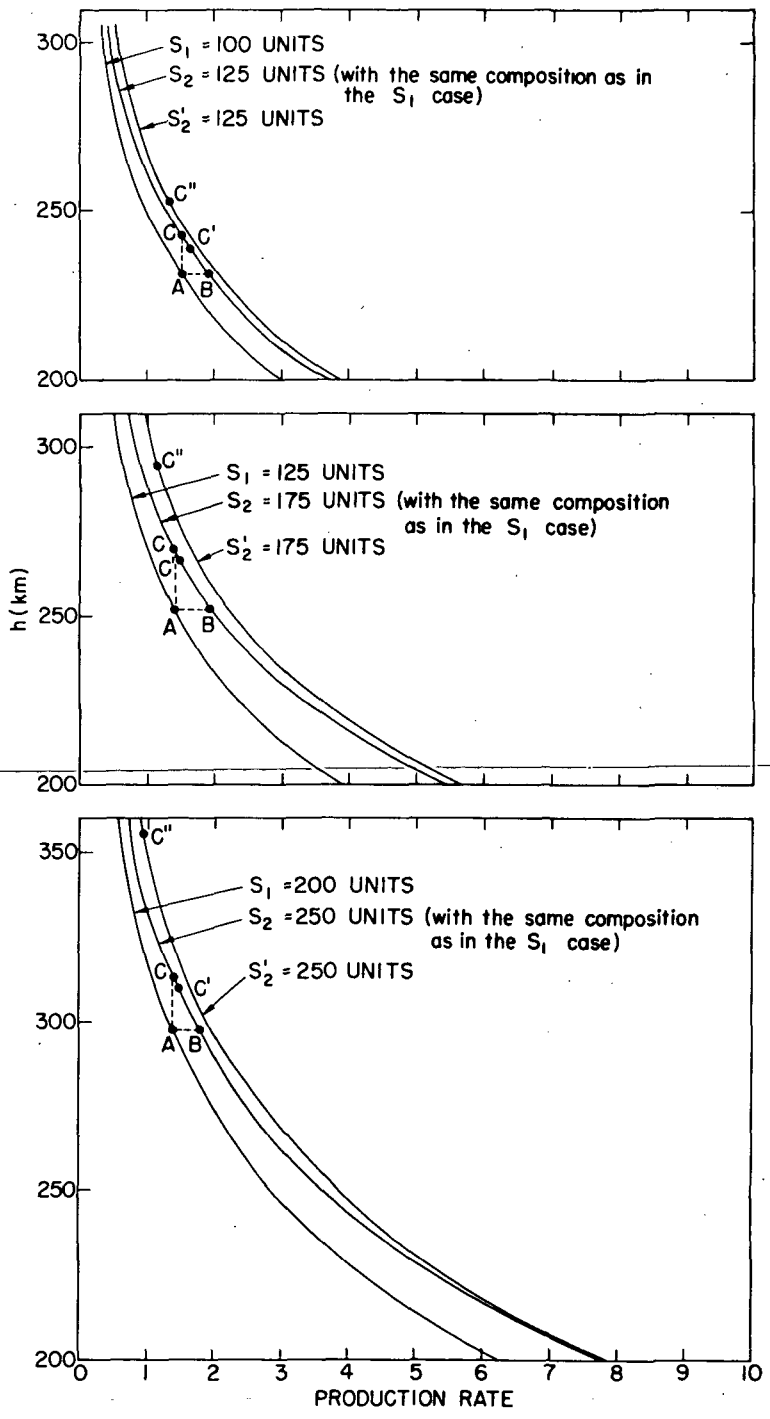

Fig. 3.2. Plots of production rates versus height for low, medium, and high solar activity, showing the equilibrium situations.

other words, when there is an increase in solar activity from S_1 to S_2, Equation (3.3) predicts a new value of production rate at the peak of the layer lying between points B and C. The new equilibrium situation found by the computer program is described by the point C' showing that, as expected, the height of the peak increased substantially; however, the value of the production rate at this height has changed only a little from its original value at A. If now one allows the neutral atmosphere to heat up under the influence of the augmented solar radiation, the gas density will increase and so will the production rate at any height. This is represented by the curve labeled S_2'. The increase in neutral temperature will reduce the pressure-gradient force and, as explained, there will be a further decrease of the wind with consequent additional rise in the layer: a new equilibrium point is found at C".

Rishbeth[op.cit. 1972] showed that, in absence of wind, the ratio β/d at the height of the peak is equal to approximately 0.6 during the daytime. When the action of neutral winds is taken into account, this ratio changes greatly and becomes a function of the solar activity.

Figure (3.3) shows the values of $\frac{\beta}{d}$ found at the height of the peak for every solar flux considered in Figures (3.2). It can be seen that when solar activity increases, that ratio decreases more and more, possibly tending towards the value of 0.6 given by Rishbeth. A best-fit curve was passed through all points in such a way to make it assymptotic to the value 0.6, i.e., for a very large solar flux, the wind effect is sufficiently small so that the value of β/d given by Rishbeth is applicable.

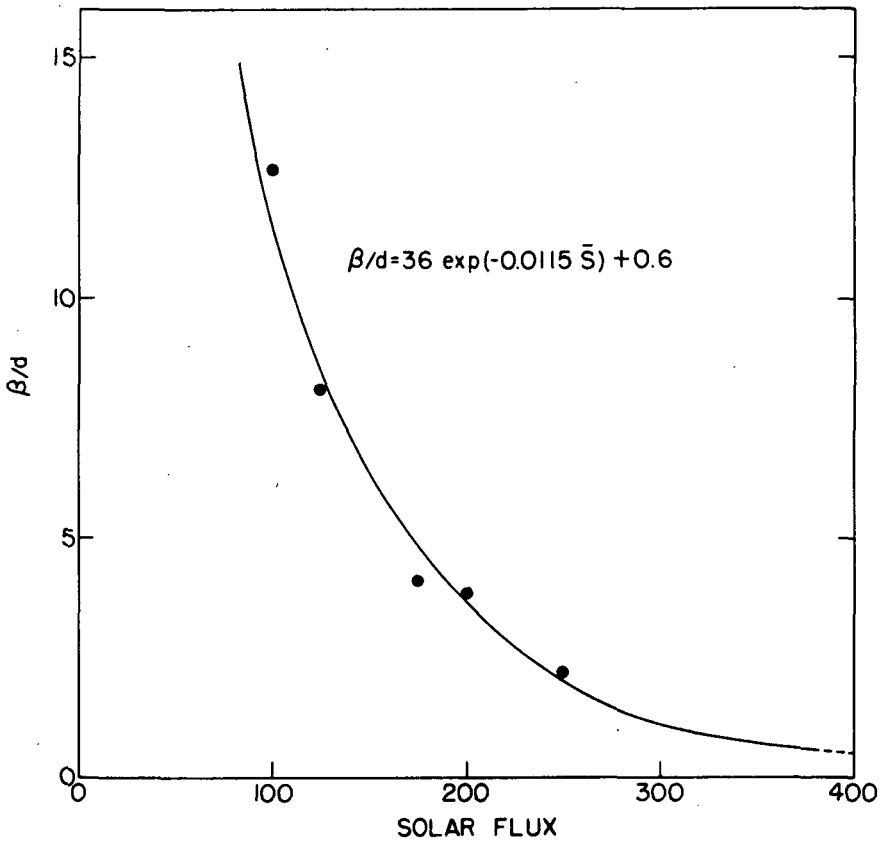

Fig. 3.3. Scatter diagram of β/d versus long-term average of the solar flux, and the corresponding best-fit curve through the scattered points which allows to define the level of occurrence of the height of the peak when the effect of neutral winds on the F2 layer is taken into consideration.

The equation of the best-fit curve is:

$$\frac{\beta}{d} = 36\exp\left(-0.0115 \times \bar{S}\right) + 0.6 \qquad (3.4)$$

This expression is valid only at the middle of the day.

The block diagram of Figure (3.4) presents in a schematic form, the feedback system just described. Box C receives as inputs informa-

tion about solar radiation, neutral temperatures (from which a neutral atmosphere concentration profile is calculated) and neutral wind profiles. The output of this box is data on ionization in the form of an N(h) profile which will be integrated between the two values of height that constitute the lower and upper boundaries of the F2-region to give the columnar electron content. The N(h) profile will also serve as an input to box B together with the neutral temperatures, used here to calculate pressure gradient forces; the output is wind velocity which completes the feedback loop to box C. Box A modifies the neutral temperatures in response to changes in solar radiation introducing a suitable delay in the process.

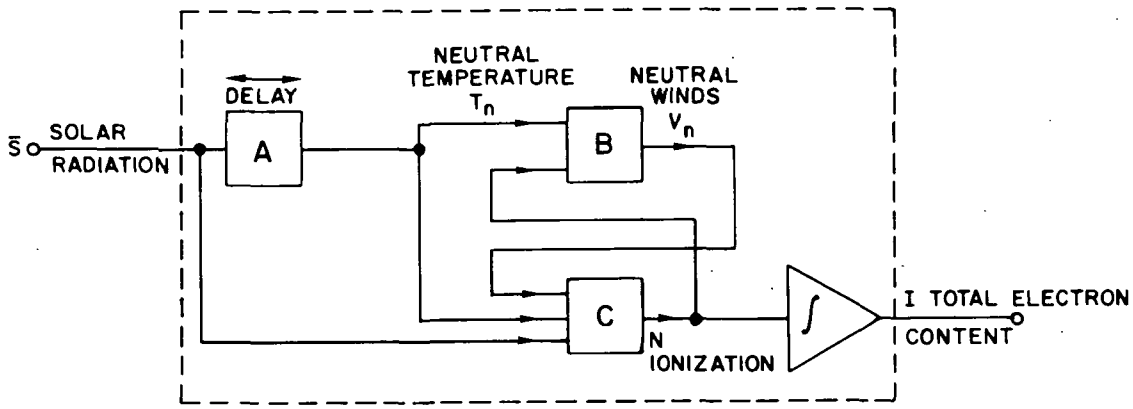

Fig. 3.4. Block diagram of the feedback system described in the text.

The response time of the ionosphere to the solar ionizing radiation is defined in the context of this work as the lag between the 27-day fluctuations in the daily average of electron content and the 27-day variations of solar decimeter flux.

Since the system of Figure (3.4), which represents the feedback mechanism described, provides a simple way for finding the output

corresponding to step functions, a sinusoidal solar input of 27-days period as that given by Equation (2.31), i.e.:

$$\bar{S} = S_0 + S_1 \cos\omega_s t$$

will be substituted by its quantized form, that is, by a series of step functions.

The smallest quantizing interval that we can take is 1 day since this time is approximately the reaction time of the neutral atmosphere to the 27-day solar input. Therefore, we have decomposed the sinusoidal solar input into 27 step functions which are shown in Figure (3.5).

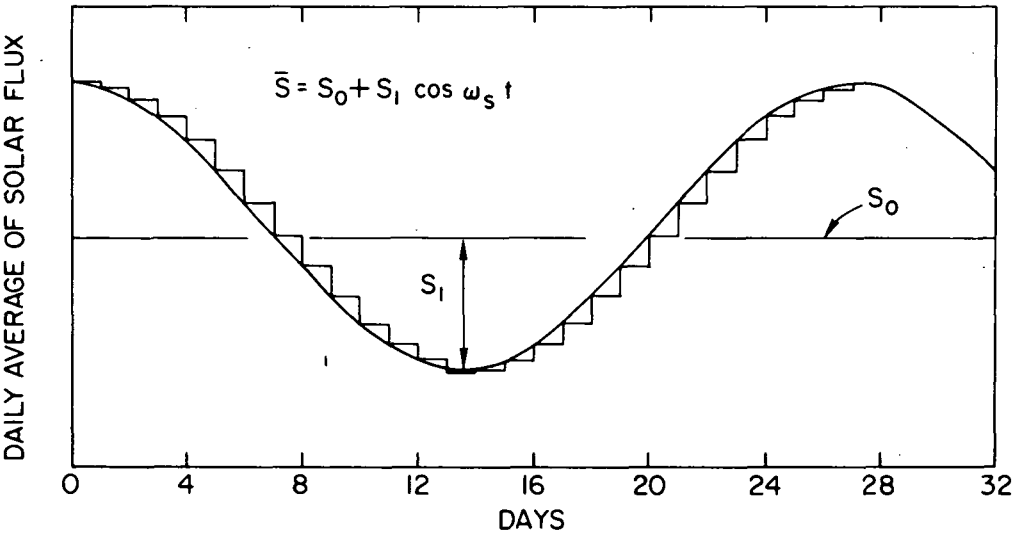

Fig. 3.5. Quantized form of the sinusoidal solar input taken at the input of the system represented in Figure (3.4).

In order to solve numerically the system represented in Figure (3.4) for the quantized solar flux applied at the input it will be useful to

express all known functions and parameters involved in the equations representing boxes A, B, and C, in terms of that input.

a) Horizontal components of the pressure-gradient force.

By definition the ξ-component of the pressure-gradient force per unit mass is:

$$F_\xi = - \frac{1}{\rho_n} \left(\frac{\partial p_n}{\partial \xi} \right) \tag{3.5}$$

where ρ_n and p_n are the density and pressure, respectively of the neutral atmosphere, and

ξ is any horizontal coordinate.

Taking the partial derivative of p_n from the perfect gas law:

$$p_n = n\ k\ T$$

where n is the neutral concentration,

k is the Boltzmann constant, and

T is the neutral temperature,

Equation (3.5) will give:

$$F_\xi = - \frac{k}{\rho_n} \left(n \frac{\partial T}{\partial \xi} + T \frac{\partial n}{\partial \xi} \right) \tag{3.6}$$

n is given by (2.23), i.e.:

$$n(h) = n(h_o) \times \frac{T(h_o)}{T(h)} \exp\left[-\int_{h_o}^{h} \frac{dh}{H(h)}\right]$$

Differentiating both sides of the above equation with respect to the independent variable ξ assuming that both $n(h_o)$ and $T(h_o)$ are independent of ξ and substituting it into (3.6) that equation is transformed into:

$$F_\xi = - T(h) \int_{h_o}^{h} \frac{g}{T^2(h)} \times \left[\frac{\partial}{\partial \xi} T(h)\right] dh \qquad (3.7)$$

Since T(h) is given by (2.24), i.e.:

$$T(h) = T_\infty - (T_\infty - T_o) \exp - \alpha(h - h_o)]$$

the derivative term of Equation (3.7) can be substituted by a more explicit form and that expression becomes:

$$F_\xi = -T(h) \times \frac{\partial T_\infty}{\partial \xi} \int_{h_o}^{h} f(h,T_\infty)\, dh \qquad (3.8)$$

where $f(h,T_\infty)$ is given by the formula:

$$f(h,T_\infty) = \frac{g}{T^2(h)} \left\{ 1 - \exp[-\alpha(h - h_o)] + \right.$$

$$\left. + (T_\infty - T_o)(h - h_o) \frac{750-1.722 \times 10^{-4}(T_\infty-800)^2}{[750+1.722 \times 10^{-4}(T_\infty-800)^2]^2} \alpha\xi \right\}$$

Equation (3.8) represents a general expression for any horizontal component of the pressure-gradient force per unit mass as a function of exospheric temperature, and height.

In order to especialize Equation (3.8) for the case of determining the two horizontal components of the pressure-gradient force corresponding to an ionospheric point P (see Fig. (3.6)) defined by the distance between the point and the center of the earth, its latitude Φ and its longitude λ we choose a coordinate system in which the x-positive is directed toward the geographic south, the y-positive, toward the geographic east and z-positive vertically upwards. In addition, the coordinate x is measured along the meridian, the coordinate y is measured along the parallel and the coordinate z radially. Therefore:

$$x = -(R_E + h)\Phi$$

$$y = \lambda(R_E + h)\cos\Phi$$

$$z = (R_E + h)$$

where R_E is the radius of the Earth, and

h the height over the surface of the earth.

On the other hand, if we assume that the geographic and geomagnetic coordinates coincide and that the frame of reference is fixed in space, i.e., it is not rotating with the earth, the longitude λ corresponding to the point P will be given by:

$$\lambda = \omega_E t$$

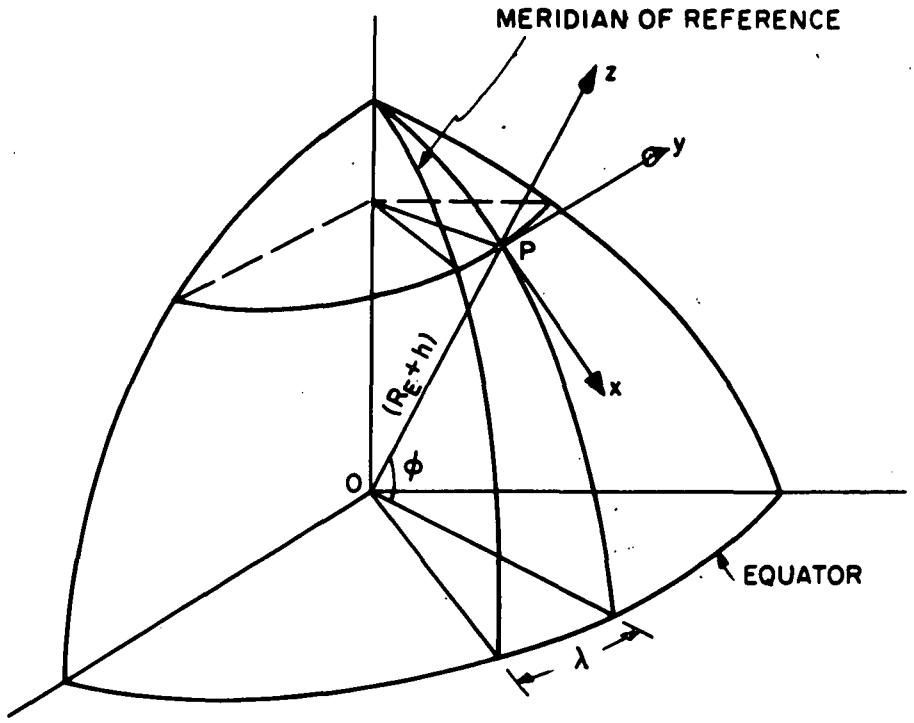

Fig. 3.6. Coordinate system used to define a given ionospheric point P, in terms of the distance between the point and the center of the earth (R_Eth), its latitude Φ, and its longitude λ.

where ω_E is the rotation frequency of the earth, and therefore, the time t and the y coordinate will be interchangeable; i.e.:

$$\frac{\partial}{\partial y} = \frac{\partial}{\partial t}\left(\frac{\partial t}{\partial y}\right)$$

or:

$$\frac{\partial}{\partial y} = \frac{1}{(R_E + h)\omega_E \cos\Phi} \frac{\partial}{\partial t}$$

similarly:

$$\frac{\partial}{\partial x} = - \frac{1}{R_E + h} \times \frac{\partial}{\partial \Phi}$$

Therefore, the two horizontal components of the pressure-gradient force expressed in terms of the exospheric temperature and height are:

$$F_x = \frac{T(h)}{R_E + h}\left(\frac{\partial T_\infty}{\partial t}\right) \int_{h_o}^{h} f(h,T_\infty)\, dh \qquad (3.9)$$

$$F_y = - \frac{T(h)}{(R_E + h)\omega_E \cos\Phi}\left(\frac{\partial T_\infty}{\partial t}\right) \int_{h_o}^{h} f(h,T_\infty)\, dh \qquad (3.10)$$

In order to express the two above equations in terms of the solar flux only, a model giving the latitude and local-time variations of the exospheric temperature was used. Such a model is that of Jacchia[1965] which is based on data obtained from observations of satellite motions and gives the following formula for the exospheric temperature:

$$T_\infty = T_{\infty_{min}} (1 + \gamma \sin^r\theta)\left(1 + \gamma \frac{\cos^r\eta - \sin^r\theta}{1 + \gamma \sin^r\theta} \cos^r \frac{\tau}{2}\right) \qquad (3.11)$$

where $T_{\infty_{min}}$ is the averaged minimum global value of the exospheric temperature (function of solar activity);

θ and η are parameters depending on latitude and solar declination;

τ is a parameter given in terms of the hour angle of the sun, that is, of the local time; and

γ and r are constants, the values of which are 0.3 and 2.5.

Equation (3.11) allows to express the two horizontal components of the pressure-gradient force, as given by (3.9) and (3.10), in terms of only the solar flux.

b) The production model.

The production of electrons and O^+ ions is caused by the photo-ionization action of the solar ultraviolet radiation. The production rate at each point of the atmosphere is given by:

$$q(h) = [O] \times \sum_{j=1}^{N_b} \sigma_{o_j}^{(i} \Phi_j \qquad (3.12)$$

where N_b is the number of bands in which the solar ultraviolet radiation has been divided;

$\sigma_{o_j}^{(i}$ is the effective ionization cross-section of the atomic oxygen in the band j;

Φ is the photon flux at level h of the atmosphere, corresponding to the band j; and

[O] is the concentration of monoatomic oxygen.

For a practical computation of q(h), the solar spectrum was divided into 16 bands. The photon fluxes and cross-sections for these intervals were taken from Garriott, da Rosa, and Davis[1969]. It was assumed that because of the rapid recombination of N_2^+ and O_2^+ ions with electrons, the ionization of N_2 and O_2 moleculars does not contribute to the total production of electrons and ions. However,the absorption of radiation by N_2 and O_2 moleculars are taken into account. Therefore:

$$\Phi_j = \Phi_{\infty_j} \exp - \left\{ \left[\tau_j(O) + \tau_j(N_2) + \tau_j(O_2) \right] \right\}$$

Φ_{∞_j} = the unattenuated photon flux at the top of the atmosphere.
$\tau_j(O)$ and $\tau_j(N_2)$ are the optical depths of O and N_2, respectively, along the path of the solar radiation, and are given by the expressions:

$$\tau_j(O) = \sigma_j^{(a}(O) \int_L n(O)\, ds \qquad (3.13)$$

$$\tau_j(N_2) = \sigma_j^{(a}(N_2) \int_L n(N_2) ds \qquad (3.14)$$

$$\tau_j(O_2) = \sigma_j^{(a}(O_2) \int_L n(O_2) ds \qquad (3.15)$$

Here, $\sigma_j^{(a}(O)$, $\sigma_j^{(a}(N_2)$, amd $\sigma_j^{(a}(O_2)$ are the corresponding absorption cross-sections.

c) The loss model.

The dominant chemical reactions involved in the loss of O^+ ions are:

$$O^+ + N_2 \rightarrow NO^+ + N \text{ with rate coefficient } \gamma_{N_2}$$

$$O^+ + O_2 \rightarrow O_2^+ + O \text{ with rate coefficient } \gamma_{O_2}$$

The loss rate of O^+ ions may be expressed:

$$\ell(h) = \gamma_{N_2}[N_2] \times [O^+] + \gamma_{O_2} \times [O_2] \times [O^+] \qquad (3.16)$$

and calling β the linear recombination coefficient, Equation (3.16) can be written $\ell(h) = \beta \times [O^+]$, where:

$$\beta = \gamma_{N_2} \times [N_2] + \gamma_{O_2} \times [O_2]$$

d) The diffusion and molecular viscosity coefficients.

For the diffusion coefficient D_p we will use the empirical formula given in the preceding chapter, i.e.:

$$D_p = 1.2 \times 10^{17} T^{0.7} / \left([O] + [N_2]\right) \quad cm^2 - sec^{-1}$$

where the neutral concentrations are given by an expression of the form (2.27), and therefore, D_p is expressed in terms of only the solar radio flux.

Similarly, the value of μ, the coefficient of molecular viscosity, is given by:

$$\mu = 4.5 \times 10^{-4}(T/1000)^{0.71} \quad \text{gr. cm}^{-1} \text{ sec}^{-1}$$

(T is given in °K in both expressions).

e) Equation of motion for the ionization.

The momentum transport equation for the O^+ ions is a mathematical expression for the sum of all forces acting over a volume element of O^+ ions moving with velocity $\vec{V}$ in a gaseous mixture of neutral particles and electrons.

Those forces are due to the pressure gradients of the O^+ ions themselves, to collisions between O^+ ions and electrons, and O^+ ions and neutral particles, to external electric, magnetic, and gravitational fields, and to the Coriolis effect. Therefore, the equation can be written:

$$\frac{d}{dt}(mN\vec{V}) = -\overline{\overline{\nabla p}} + Ne(\vec{E} + \vec{V} \times \vec{B}) - mN\nu_{ie}(\vec{V} - \vec{v}_e) - mN\nu_{in}(\vec{V} - \vec{v}_n) + mN\vec{g} + 2mN(\vec{V} \times \omega_E) \qquad (3.17)$$

where m = mass of the O^+ ions,

N = concentration of the O^+ ions,

$p = NkT_i$

$\vec{E}$ = the electric field

$\vec{B}$ = the geomagnetic flux density ($-B\cos\Psi$, 0, $-B\sin\Psi$) with Ψ the

dip angle,

υ_{ie} and υ_{in} are the effective collision frequencies between ions and electrons and ions and neutrals, respectively,

$\vec{V}_e$ = bulk electron velocity,

$\vec{V}_n$ = bulk neutral particles velocity,

$\vec{g}$ = acceleration due to gravity (0, 0, -g),

$\vec{\omega}_E$ = Earth's rotation frequency, and

$\vec{V}$ = bulk ion velocity.

Neglecting the frictional force between O^+ ions and electrons, the Coriolis and the acceleration terms because of their small magnitude (Rishbeth[op.cit.1972]) Equation (3.17) becomes:

$$0 = -k\overrightarrow{\nabla(NT_i)} + Nm\vec{g} + eN(\vec{E} + \vec{V} \times \vec{B}) - Nm\upsilon_{in}(\vec{V} - \vec{v}_n) \quad (3.18)$$

Equation (3.18) also applies to the electron motion and, neglecting small terms which involve the electron mass, one obtains:

$$0 = -k\overrightarrow{\nabla(NT_e)} - eN(\vec{E} + \vec{v}_e \times \vec{B}) \quad (3.19)$$

With the purpose of facilitating the solution of the two last equations it will be convenient to express them in terms of the diffusion velocity, $\vec{V}_d$, which represents either the ion or electron velocity when the neutral air is at rest. This means that under these conditions electrons would interact with the ions only via the electric field.

Therefore, assuming in (3.18) and (3.19) that:

$$\vec{V}_d = \vec{V} = \vec{v}_e$$

and:

$$\vec{v}_n = 0$$

we will have:

$$\vec{V}_d = -\frac{\vec{g}}{\nu_{in}} - \frac{k}{m\nu_{in}}\left[\frac{1}{N}\nabla(\vec{N}T_i) + \frac{1}{N}\nabla(\vec{N}T_e)\right]$$

Defining the plasma temperature, T_p, the plasma diffusion coefficient, D_p, and its scale height, H_p, by the equations:

$$T_p = \frac{T_e + T_i}{2}$$

$$D_p = \frac{2kT_p}{m\nu_{in}}$$

$$H_p = \frac{kT_p}{mg}$$

we can express the drift velocity of the plasma, v_d, by the well-known equation:

$$v_d = -D_p\left(\frac{1}{2H_p} + \frac{1}{T_p}\frac{\partial T_p}{\partial Z} + \frac{1}{N}\frac{\partial N}{\partial Z}\right) \qquad (3.20)$$

Now the solution of the six scalar equations resulting from the two vectorial equations (3.18) and (3.19) is carried out in an analytical way, giving for the three components of the ion velocity:

$$V_x = v_{nx} \cos^2\Psi + v_{nz} \sin\Psi \cos\Psi + V_{\perp x} \qquad (3.21)$$

$$V_y = V_{\perp y} - v_{nz} \cos\Psi \qquad (3.22)$$

$$V_z = v_d \sin^2\Psi + v_{nx} \sin\Psi \cos\Psi + v_{nz} \sin^2\Psi + V_{\perp z} \qquad (3.23)$$

where $V_{\perp x}$, $V_{\perp y}$, and $V_{\perp z}$ are the three components of the drift velocity caused by the electric field. Under quiet conditions, small geomagnetic disturbance index, these drifts are small compared with the drift caused by the neutral winds as it was pointed out in the preceding chapter and therefore, they will be disregarded in further calculations.

f) Equation of motion for the neutral air.

The balance of forces is established between actions due to inertial plus Coriolis opposing to the summation of the actions due to pressure-gradient, ion-drag, gravity, and viscosity. Therefore, the equation of motion of the neutral air, after having neglected the grad-force due to the collisions between neutral particles and electrons, takes the form:

$$\frac{\vec{dv}_n}{dt} + 2\vec{\omega}_E \times \vec{v}_n = \vec{F} + \vec{g} + \frac{\mu}{\rho}\vec{\nabla^2 v}_n + \frac{N\nu_{in}m}{\rho}(\vec{V} - \vec{v}_n) \qquad (3.24)$$

where ρ is the density of the neutral atmosphere.

The first term on the l.h.s. of the above equation will be neglected in the steady-state solution used throughout this investigation; besides its small magnitude compared with that of the Coriolis term, as discussed by Geisler[op.cit. 1966] and Kohl and King[1967], makes it negligible even for time-varying solutions of that equation.

In addition, the vertical component of the vectorial Equation (3.24) virtually reduces to the hydrostatic equation $F_z = g$ because the vertical component of the Coriolis term is of order $10^{-3} \times g$ and the other terms are smaller still (Rishbeth[op.cit. 1972]). Therefore, only the two horizontal components of the equation will be considered.

Calling $f_c = 2\omega_E \sin\Phi$, the Coriolis parameter, and $f_d = KN$, the ion-drag parameter, the two scalar equations take the form:

$$\frac{\mu}{\rho} \frac{\partial^2 v_{nx}}{\partial Z^2} + f_c v_{ny} - f_d v_{nx} \sin^2\Psi + F_x = 0 \qquad (3.25)$$

$$\frac{\mu}{\rho} \frac{\partial^2 v_{ny}}{\partial Z^2} - f_c v_{nx} - f_d v_{ny} + F_y = 0 \qquad (3.26)$$

which must be solved for v_{nx} and v_{ny}.

g) Equation of continuity.

The continuity equation, as it was analyzed in the preceding chapter can be written, under steady-state conditions, and assuming that the spatial variations of the derivative term are much more gradual in the horizontal plane than in the vertical:

$$q = \beta N + \frac{\partial}{\partial Z}(NV_z)$$

Calling: $$W_d = v_d \sin^2\Psi$$

$$W_n = v_{nx} \sin\Psi \cos\Psi$$

the vertical drifts caused by diffusion and neutral winds, respectively and:

$$W_T = W_d + W_n$$

the continuity equation may be written:

$$q = \beta N + N\frac{\partial W_T}{\partial Z} + W_T \frac{\partial N}{\partial Z} \qquad (3.27)$$

which, together with (3.25) and (3.26) will be solved in the next chapter for the electron concentration profile, N(h), and the wind velocity $\vec{v}_n(h)$.

CHAPTER 4

NUMERICAL METHOD AND BOUNDARY CONDITIONS

In the solution of the system discussed in the preceding chapter, the equations involved are those labeled (3.20), (3.25), (3.26), and (3.27); i.e.:

$$v_d = -D_p\left(\frac{1}{2H_p} + \frac{1}{T_p}\frac{\partial T_p}{\partial Z} + \frac{1}{N}\frac{\partial N}{\partial Z} \right) \qquad (3.20)$$

$$\frac{\mu}{\rho}\frac{\partial^2 v_{nx}}{\partial Z^2} + f_c v_{ny} - f_d v_{nx} \sin^2\Psi + F_x = 0 \qquad (3.25)$$

$$\frac{\mu}{\rho}\frac{\partial^2 v_{ny}}{\partial Z^2} - f_c v_{nx} - f_d v_{ny} + F_y = 0 \qquad (3.26)$$

$$q = \beta N + N\frac{\partial W_T}{\partial Z} + W_T\frac{\partial N}{\partial Z} \qquad (3.27)$$

Rishbeth and Barron[op.cit.1960] developed a technique to solve simultaneously Equations (3.20) and (3.27), i.e., to solve the above problem disregarding the action of the neutral wind. The same technique can be applied to the present situation if the viscosity terms are neglected. Equations (3.25) and (3.26) are then reduced to algebraic rather than differential equations and, by combining them with (3.27) v_{nx} and v_{ny} can be eliminated leaving a pair of simultaneous first-order differential equations.

The effect of neglecting the viscosity terms is not important at low levels, say up to about 300 km, because at such heights neutral winds are largely controlled by the Coroilis and ion-drag forces and the viscosity effect is negligible. At greater heights the opposite occurs, i.e., the rapid upward decrease of the density ρ causes the viscosity term to dominate the equation of air motion.

In order to estimate the magnitude of the viscous term let us consider a range of heights in which this term greatly exceeds all others in the equation of motion, which then can be written:

$$\frac{\mu}{\rho}\left(\frac{\partial^2 v_n}{\partial z^2}\right) = 0 \qquad (4.1)$$

where v_n represents either v_{nx} or v_{ny}.

Since ρ varies with height much faster than μ, we will assume that only the former parameter is height dependent. Therefore:

$$\frac{\partial}{\partial z}\left(\frac{\mu}{\rho}\frac{\partial v_n}{\partial z}\right) = -\frac{\mu}{\rho}\left(\frac{\partial \rho}{\partial z}\right)\left(\frac{\partial v_n}{\partial z}\right) + \frac{\mu}{\rho}\left(\frac{\partial^2 v_n}{\partial z^2}\right) \qquad (4.2)$$

The second term on the r.h.s. of Equation (4.2) was assumed to be zero (Equation (4.1)), and since the variation of ρ with height is of the form:

$$\rho \propto \exp\left(-\frac{h}{H}\right)$$

Equation (4.2) becomes:

$$\frac{\partial}{\partial z}\left(\frac{\mu}{\rho}\frac{\partial v_n}{\partial z}\right) = \frac{\mu}{\rho H}\left(\frac{\partial v_n}{\partial z}\right)$$

or:

$$\frac{d\left[\frac{\mu}{\rho}\left(\frac{\partial v_n}{\partial z}\right)\right]}{\frac{\mu}{\rho}\left(\frac{\partial v_n}{\partial z}\right)} = \frac{dz}{H}$$

and integrating once this last equation, one finds that:

$$\frac{\partial v_n}{\partial z} \propto \exp\left(\frac{h}{H}\right) \qquad (4.3)$$

If the derivative of v_n varies according to (4.3), v_n will vary following the same law, consequently the terms:

$$\frac{\mu}{\rho}\left(\frac{\partial^2 v_{nx}}{\partial z^2}\right)$$

and:

$$\frac{\mu}{\rho}\left(\frac{\partial^2 v_{ny}}{\partial z^2}\right)$$

in Equations (3.25) and (3.26) can be replaced by the approximate values:

$$\frac{\mu}{\rho H^2} v_{nx}$$

and:

$$\frac{\mu}{\rho H^2} v_{ny}$$

Since f_c, the Coriolis parameter, is independent of height, com-

paring at every height $\mu/\rho H^2$ with f_d, the ion-drag parameter, it is possible to determine the height at which the viscosity dominates. From that height up to the top of the ionosphere, the neutral wind velocity is taken independent of height because in that range the velocity gradient must tend to zero otherwise the viscosity would become overwhelmingly large.

In view of the above, the viscosity effect will be considered indirectly as a boundary condition imposed on the neutral wind profile obtained by integrating the following pair of equations:

$$w_d = - D_a \left(\frac{1}{2H\rho} + \frac{1}{T_p} \frac{\partial T_p}{\partial z} + \frac{1}{N} \frac{\partial N}{\partial z} \right) \qquad (4.4)$$

$$q = \beta N + N \frac{\partial}{\partial z} \left(w_d + w_n \right) + \left(w_d + w_n \right) \frac{\partial N}{\partial z} \qquad (4.5)$$

where: $$D_a = D_p \sin^2 \Psi$$

and: $$w_n = \frac{f_d F_x + f_c F_y}{f_c^2 + f_d^2 \sin^2 \Psi} \sin \Psi \cos \Psi$$

The computer program for solving Equations (4.4) and (4.5) includes a series of subroutines which allow the calculation, as discussed in the preceding chapter, of the parameters D_a, H_p, T_p, q, β, F_x in terms of height for every solar input. The derivative terms $\frac{\partial T_p}{\partial z}$ and $\frac{\partial w_n}{\partial z}$ are approximated by the finite difference equivalents; i.e., at the j^{th} step of integration, these terms are:

$$\left(\frac{\partial w_n}{\partial z}\right)_j = \frac{w_{n_{j+1}} - w_{n_{j-1}}}{2\Delta h}$$

$$\left(\frac{\partial T_p}{\partial z}\right)_j = \frac{T_{p_{j+1}} - T_{p_{j-1}}}{2\Delta h}$$

We set the lower boundary at the height h_0 = 120 km and the upper boundary at h_∞ = 600 km. At the lower boundary we assume that the electron concentration N_0 and the neutral wind velocity $\vec{v}_{n_0}$ are identically equal to zero. The upper boundary condition for ionization is that the diffusive flux of ionization vanishes at the top of the ionosphere, i.e.:

$$\left(Nw_d\right)_{z=h_\infty} = 0 \qquad (4.6)$$

The height interval between h_0 and h_∞ is divided into n steps such that:

$$n = \frac{h_\infty - h_0}{\Delta h} + 1$$

where Δh is the height-step chosen, taken to be 5 km throughout all these calculations.

The upper boundary condition can be satisfied for any arbitrary value of the electron concentration by simply setting

$$\left(w_d\right)_{z=h_\infty} = 0$$

However, since the solution proceeds downwards through the ionosphere step by step the value of the electron concentration found at the lower boundary will not, in general, satisfy the lower boundary condition of,

$$(N)_{z=h_0} = 0$$

The only way in which both boundary conditions can be met is by a series of systematic trials. The possible types of behavior which may arise are illustrated in Figure (4.1).

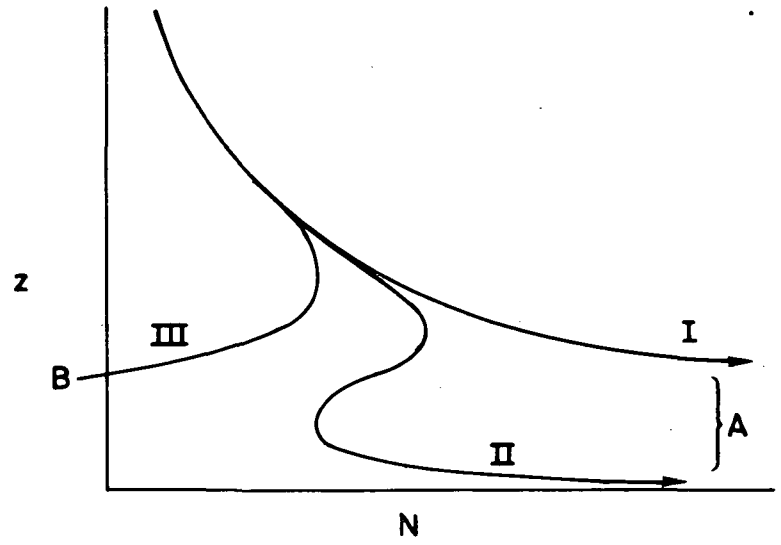

Fig. 4.1. Types of behavior of the computed electron concentration distributions N(h).

Solution I leads to exaggerated values of N. Solution II also leads to excessive values of N, but first it passes through a local maximum of electron concentration. Solution III leads to negative values of N.

Solutions I and II stand for "condition A" (excessive values of N) and Solution III stands for "condition B" (low values of N).

TABLE 2

CONDITION	DECISION
Was 0	
Changes to A	$(N)_{z=h_\infty} \rightarrow (N)_{z=h_\infty} - \Delta N$
Changes to B	$(N)_{z=h_\infty} \rightarrow (N)_{z=h_\infty} + \Delta N$
Was A	
Remains in A	$(N)_{z=h_\infty} \rightarrow (N)_{z=h_\infty} - \Delta N$
Changes to B	$(N)_{z=h_\infty} \rightarrow (N)_{z=h_\infty} + \Delta N \ (\Delta N \rightarrow \Delta N/10)$
Was B	
Changes to A	$(N)_{z=h_\infty} \rightarrow (N)_{z=h_\infty} - \Delta N \ (\Delta N \rightarrow \Delta N/10)$
Remains in B	$(N)_{z=h_\infty} \rightarrow (N)_{z=h_\infty} + \Delta N$

The first passage through the computer will be called "Condition 0". Boolean comparisons in the computer recognize the corresponding condition. Hence, if a condition was the so-called 0 and went to condition A, the electron concentration $(N)_{z=h_\infty}$ was excessive and a new attempt is made with

$$(N)_{z=h_\infty} \rightarrow (N)_{z=h_\infty} - \Delta N$$

where ΔN is the increment of electron concentration introduced in the program.

It should be remembered that all parameters involved in Equations (4.4) and (4.5) can be expressed as functions of the solar radio flux, $\bar{S}$, only. Thus, specifying $\bar{S}$ specifies a complete electron concentration profile and the corresponding neutral wind profile. The two equations were solved using the procedure described above, applying a collection of values of $\bar{S}$ taken from the expression:

$$\bar{S} = 100 + 15 \cos\omega_s t \qquad (4.7)$$

Here, we have chosen a situation in which the long term average value of solar flux is 100 units and, in the nomenclature of Chapter 2, the parameter D_s is taken as equal to 0.15. The choice of these values allows the comparison of the results of this Chapter with those of Chapter 2. Thirty-one consecutive values of $\bar{S}$ were used as the quantized waveform at the input of the system described in detail in Chapter 3. All parameters were calculated for the autumnal equinox. The result is shown in Figure (4.2) which represents the above solar input and the corresponding electron content with its best-fit. From this it was found that the sensitivity and the delay corresponding to the electron content are:

$$D_I = 0.5$$

δ_I = 2.6 days

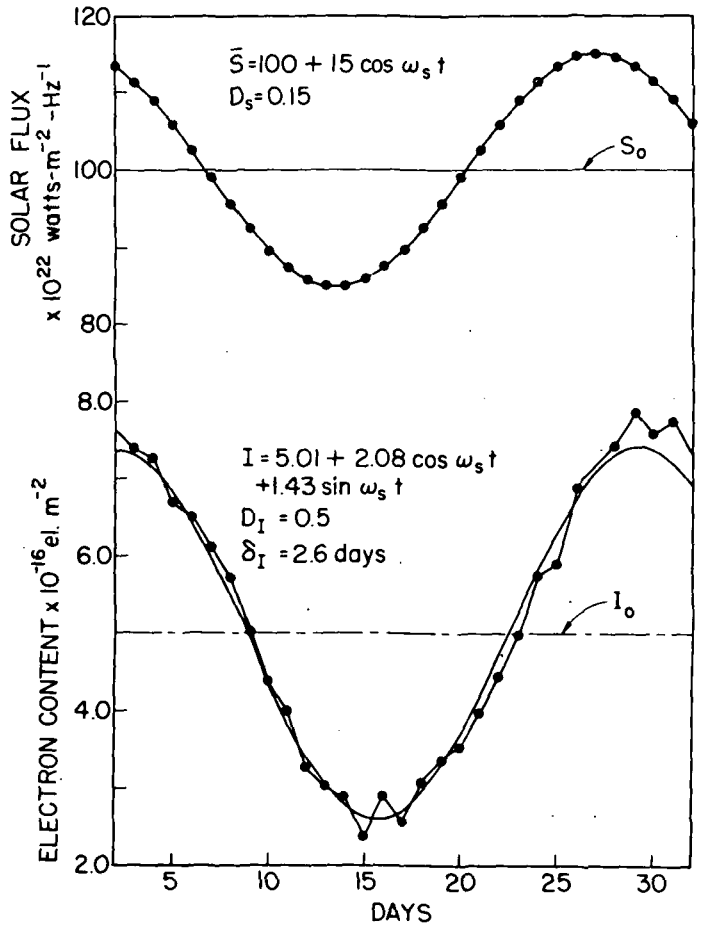

Fig. 4.2. Solar input and the corresponding electron content with its best-fit, calculated from the theoretical model described in the text.

The noise which appears in the computed electron content is probably a consequence of a constraint introduced into the program, with the purpose of saving computer time: the electron content computed at every step is stored before the iterative process converges fully. Nevertheless, the total amount of computer time necessary is very considerable,

suggestive of further simplifications.

If the system discussed in Chapter 3 is assumed to be linear with only minor linearities left, a simpler technique can be used for the special purpose of determining the sensitivity and delay corresponding to the electron content. The technique consists of decomposing the sinusoidal input in a series of rectangle functions, as shown in Figure (4.3); every one of which produces at the output of the system a waveform with its center of gravity shifted with respect to the input. Calculating the response corresponding to a given input rectangle function, the others can be inferred from linearity considerations.

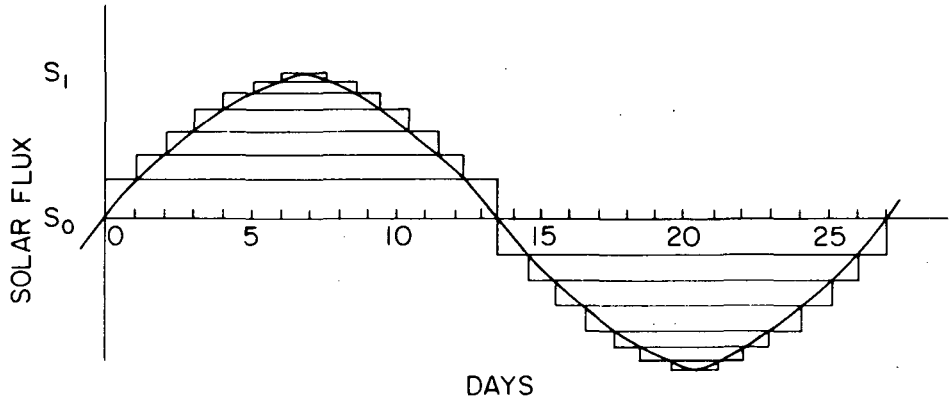

Fig. 4.3. Series of rectangle functions taken as an approximation of the sinusoidal solar flux of 27-days period.

Calling A_i and δ_i the area and shift, respectively, corresponding to the output waveform caused by the i^{th} input rectangle, the total shift, i.e., the delay between the output and the input is defined by:

$$\delta_I = \frac{\sum_{i=0}^{6} A_i \delta_i}{\sum_{i=0}^{6} A_i} \qquad (4.8)$$

Equation (4.8) implies the use of the superposition theorem, i.e., that the system considered is nearly linear.

When this technique was applied to the solar input given by Equation (4.7) the sensitivity and delay found corresponding to the electron content were:

$$D_I = 0.474$$

$$\delta_I = 2.72 \text{ days}$$

which suggests that the assumption made about the linearity of the system does not depart much from reality when the system is considered as a simulation of the ionosphere under low geomagnetic activity conditions and with a sinusoidal solar input. As a matter of fact, it is shown in Chapter 5, where experimental observations are examined, that in periods when the geomagnetic disturbance index is small the sinusoidal solar input of 27-day period causes a sinusoidal behavior in the corresponding electron content, with the same period.

The computer time needed when these assumptions are made represents about 32% of the computer time needed when the quantizing technique is applied.

Therefore, it was decided to apply the approximate technique to several values of solar flux, with the purpose of covering the range of variation of solar activity. The results are displayed in Table 3.

TABLE 3

$D_s = 0.15$

S_o	δ_I	D_I
80	3.46	0.481
100	2.72	0.474
150	1.80	0.414
200	1.38	0.372

Using the values of S_0 and δ_I shown in Table 3, a best-fit exponential curve was calculated which allows for writing the following expression:

$$\delta_I = 6 \exp(-0.0075 \times S_0) \quad \text{days} \qquad (4.9)$$

The comparison of these results with those found in Chapter 2, leads to the following conclusions:

a) The delay of the electron content decreases when solar activity increases, whether or not the neutral wind effect is considered. However, under low solar activity conditions, when the neutral wind effect is more important and therefore the feedback mechanism described more powerful, the variation between the delay calculated when the wind effect is considered and the delay calculated when the wind effect is neglected is much larger than the same variation calculated under high solar activity conditions.

b) The sensitivity of the electron content, i.e. the ratio between

the amplitude of the a.c. component and the d.c. term, is larger for all solar activity levels than the equivalent parameter, i.e. D_s, corresponding to the solar flux. Nevertheless, as a consequence of the feedback mechanism which increases the sensitivity of the electron content, the conclusion found in Chapter 2 concerning the increase of sensitivity with solar activity now is modified in the sense that the sensitivity of the electron content decreases when solar activity increases, because the feedback mechanism is more powerful under low solar activity conditions.

CHAPTER 5

OBSERVATIONS

In this chapter a statistical analysis of data is carried out looking for a quantitative measure of the ionospheric response to the the 27-day variations of the solar input. Specifically, we are interested in determining the delay of the response of the electron content to fluctuations in the solar flux as well as the magnitude of the electron content fluctuation for a given change in solar flux.

Since the 27-day effect is not the only information present in the data corresponding to either the solar flux or the electron content, it is crucial to isolate that effect from others. With that purpose we will consider the 27-day effect present in the data as a periodic signal and the rest as a random noise.

The strong fluctuations observed in the day-to-day variations of the daily average electron content will be smoothed out by passing the data through a mathematical 7-days running mean filter which does not introduce any phase changes and causes very small attenuation to the 27-days period component.

Calling $\hat{I}$ and $\hat{S}$ the estimated values of electron content and of solar flux, respectively, i.e., the values derived from the best-fit made over the actual data, we can represent them by the equations:

$$\hat{I} = I_o + A_I \cos(\omega_s t - \Phi_I) \qquad (5.1)$$

$$\hat{S} = S_o + A_S \cos(\omega_s t - \Phi_S) \qquad (5.2)$$

where $I_o, A_I, \Phi_I, S_o, A_S$ and Φ_S are calculated with the least squares

criterion. Once the phases Φ_I and Φ_S are determined, the delay of the electron content is given by:

$$\delta_I = \frac{1}{\omega_s} (\Phi_I - \Phi_S) \text{ days} \qquad (5.3)$$

In addition, we define:

$$\sigma_S^2 = \overline{(S - \hat{S})^2} \qquad (5.4)$$

as the variance of the solar flux S, and

$$\sigma_I^2 = \overline{(I - \hat{I})^2} \qquad (5.5)$$

as the variance of the corresponding electron content.

Further we assume that everyone of the calculated amplitudes, A_S or A_I, results from the superposition of an amplitude, namely a_S or a_I, due to the 27-day variation, and an additional term, A_{R_S} or A_{R_I}, resulting from the best-fitting over a random set of points equally spaced. The magnitude of this additional term is related to the dispersion around the mean of the points over which the best-fit was performed, i.e., to σ_S or σ_I.

In order to find the relationship between the amplitude of the additional term and the corresponding standard deviation, let us consider N_p consecutive values, equally spaced, of a random variable y such that:

$$y = x - \hat{x} \qquad (5.6)$$

where x represents a random variable (say S or I) and $\hat{x}$ its estimate value.

The variance of y is, by definition:

$$\sigma_y^2 = \overline{y^2} - \overline{y}^2 \qquad (5.7)$$

But $\overline{y} = 0$ as a consequence of the least squares criterion applied to calculate the estimate value of x. Therefore, the second term on the r.h.s. of Equation (5.7) vanishes. Substituting (5.6) into (5.7) and considering that according to either (5.4) or (5.5)

$$\sigma_x^2 = \overline{(x - \hat{x})^2}$$

one finds that:

$$\sigma_y = \sigma_x \qquad (5.8)$$

On the other hand, if a sinusoid

$$R \cos(\omega_s t - \Phi_R)$$

is fitted through the N_p consecutive values of y, the best-fitting condition with the least -squares criterion implies that the expression:

$$\sum_{i=1}^{N_p} \left[y_i - R \cos(\omega_s t - \Phi_R) \right]^2$$

must be a minimum.

In the preceding equations, R is the random amplitude of the sinusoidal term, and Φ_R is the phase of the sinusoidal term. This phase is

assumed to be a random variable uniformly distributed between 0 and 2π, and statistically independent of R.

Taking the derivative of the above expression with respect to R and equating it to zero, as required by the existence of a minimum, one finds that

$$R = \frac{\sum_{i=1}^{N_p} y_i \cos(\omega_s t - \Phi_R)}{\sum_{i=1}^{N_p} \cos^2(\omega_s t - \Phi_R)}$$

The amplitude of the additional term is defined as the r.m.s. of R, i.e.:

$$A_R = \sqrt{\frac{\sum_{i=1}^{N_p} \overline{y_i^2 \cos^2(\omega_s t - \Phi_R)}}{\sum_{i=1}^{N_p} \overline{\cos^4(\omega_s t - \Phi_R)}}} \qquad (5.9)$$

Calling:

$$\overline{P} = \sum_{k=1}^{N_p} \overline{y_k \cos\theta_k} = \sum_{k=1}^{N_p} \overline{y_k} \times \overline{\cos\theta_k}$$

its square mean will be:

$$\overline{P^2} = \sum_{k=1}^{N_p} \sum_{\ell=1}^{N_p} \overline{y_k y_\ell} \times \overline{\cos\theta_k \cos\theta_\ell}$$

$$= \sum_{\substack{k=1 \\ (k=\ell)}}^{N_p} \overline{y_k^2} \times \overline{\cos^2\theta_k} + \sum_{k=1}^{N_p} \sum_{\substack{\ell=1 \\ (k \neq \ell)}}^{N_p} \overline{y_k} \times \overline{y_\ell}\ \overline{\cos\theta_k} \times \overline{\cos\theta_\ell}$$

The second term on the r.h.s. of the last expression vanishes, and

$$\overline{\cos^2\theta_k} = \frac{1}{2}$$

Therefore:

$$\overline{p^2} = \frac{N_p}{2}\sigma_y^2 \qquad (5.10)$$

Substituting this result in (5.9), after taking account (5.8), the amplitude of the additional term is given by:

$$A_R = \sqrt{\frac{2}{N_p}}\ \sigma_x$$

Therefore:

$$A_{R_S} = \sqrt{\frac{2}{N_p}}\,\sigma_S \qquad (5.11)$$

and

$$A_{R_I} = \sqrt{\frac{2}{N_p}}\,\sigma_I \qquad (5.12)$$

The error distribution in phase can be found with the aid of the Figure(5.1) which represents the triangle formed by the three amplitudes involved; i.e., the amplitude of the additional term, A_R, taken with a random phase θ assumed to be uniformly distributed between 0 and 2π, the amplitude caused by the 27-day period component present in the data, a_x, and the resultant of both, the calculated amplitude, A_x.

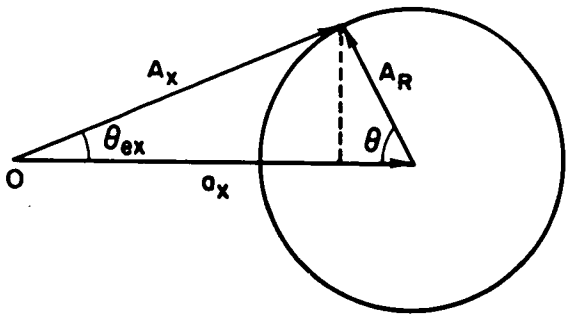

Fig. 5.1. Sketch of the amplitude measured, A_x, resulting from the geometrical addition of the amplitude caused by the 27-days effect, a_x, and the amplitude of the random term, A_R.

The angle θ_{e_x} represents the error in phase with which A_x is taken at the moment considered in Figure(5.1). It is given by:

$$\theta_{e_x} = \arcsin\left(\frac{A_R \sin\theta}{A_x}\right) \qquad (5.13)$$

And calling:

$$g_x = \frac{A_x}{A_R}$$

the signal-to-noise ratio, the mean value of θ_{e_x} can be written,

$$\overline{\theta}_{e_x} = \frac{27}{2\pi^2} \int_0^{\pi} \arcsin\left(\frac{\sin\theta}{g_x}\right) d\theta \quad \text{days}$$

Therefore, the dispersion in phase will be:

$$\bar{\theta}_{e_T} = \sqrt{\bar{\theta}^2_{e_S} + \bar{\theta}^2_{e_I}} \qquad (5.15)$$

The sensitivity of the electron content for a given variation of the solar flux is defined:

$$\gamma = \left(\frac{A_I}{I_o}\right) \Big/ \left(\frac{A_S}{S_o}\right) \qquad (5.16)$$

but, according to (5.14), (5.11), and (5.12) the signal-to-noise ratios corresponding to the solar flux and to the electron content are:

$$g_S = \sqrt{\frac{N_p}{2}} \left(\frac{A_S}{\sigma_S}\right) \qquad (5.17)$$

and:

$$g_I = \sqrt{\frac{N_p}{2}} \left(\frac{A_I}{\sigma_I}\right) \qquad (5.18)$$

Therefore, eliminating A_S and A_I from the last three expressions, Equation (5.16) can be written:

$$\gamma = \left(\frac{g_I}{g_S}\right)\left(\frac{d_I}{d_S}\right) \qquad (5.19)$$

where d_I and d_S are called deviation indices, defined by the expressions

$$d_I = \frac{\sigma_I}{I_o}$$

$$d_S = \frac{\sigma_S}{S_o}$$

A computer program was prepared, which, using data corresponding to the year of 1969 for stations at Stanford ATS-1 and ATS-3, Hawaii, Cold Bay, Fort Collins, Rosman, Edmonton, and Urbana, calculates for every 32 consecutive values of S and I, and with a sliding interval of 5 days, the set of values given by the expressions (5.1), (5.2), (5.3), (5.4), (5.12), (5.17), (5.18), and (5.19) as well as the cross-correlation function, for different time-shifts, between the solar flux and the electron content data.

The reason why 1969 was chosen is that during that year the 10.7 cm solar flux exhibited well developed fluctuations with periods of about 27-days and with a long-term component fairly constant, as seen in Figure (5.2).

Defining the total signal-to-noise ratio, g_T, as the square root of the product of the signal-to-noise ratios corresponding to the solar flux and to the electron content, i.e.,

$$g_T = (g_S \times g_I)^{1/2} \qquad (5.20)$$

it was possible to plot this parameter throughout the year period considered.

When the signal-to-noise ratio as defined above, exceeds some arbitrarily chosen level one can expect that the phenomena observed are dominated by solar flux fluctuations and the measured delays can be compared with the theoretical ones computed in Chapter 4.

The major degradations of signal-to-noise ratio appear to be

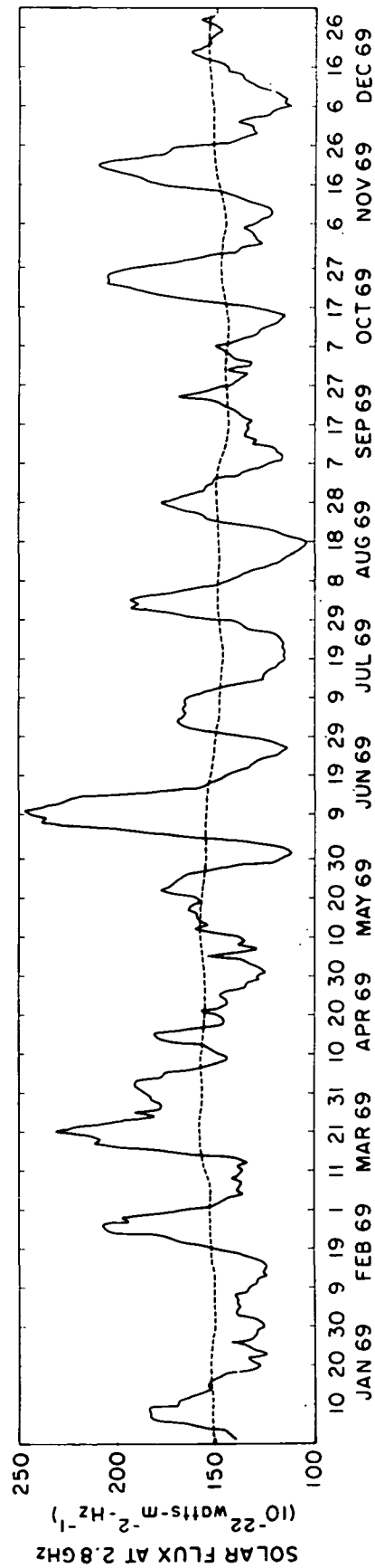

Fig. 5.2. Variation of the solar radio flux at 2.8 GHz (Ottawa), throughout the year of 1969.

associated with geomagnetic disturbances as can be seen from Figure(5.3) in which the geomagnetic disturbance index, A_p, is plotted together with g_T corresponding to the eight stations mentioned above. It can be seen that there is a clear anticorrelation between these quantities. The discontinuities that appear in some g_T curves are caused by gaps in the data.

The effect of variations in the geomagnetic disturbance index on the ionospheric response can be seen by comparing the plots corresponding to the delay and sensitivity functions derived from equations (5.3) and (5.19), respectively, against the plot representing the geomagnetic disturbance index.

If the delay derived from Equation (5.3) is compared with that associated with the maximum of the correlation coefficient between the solar flux and the electron content, one finds that they coincide with one another during periods of low geomagnetic activity index. During disturbed periods there is a discrepancy between the two delays but they follow the same general trend.

Figures (5.4a) and (5.4b) represent two sets of delays and sensitivity functions corresponding to Stanford ATS-1 and Hawaii stations, respectively. Neither of these stations present any long gap in the data and therefore the functions plotted are continuous throughout the period considered. They are representative of the behavior of other stations and lead to the conclusion that the actual value of the time-delay between the electron content and the 27-days period fluctuations in solar activity can be observed only if the solar flux exhibits a well developed

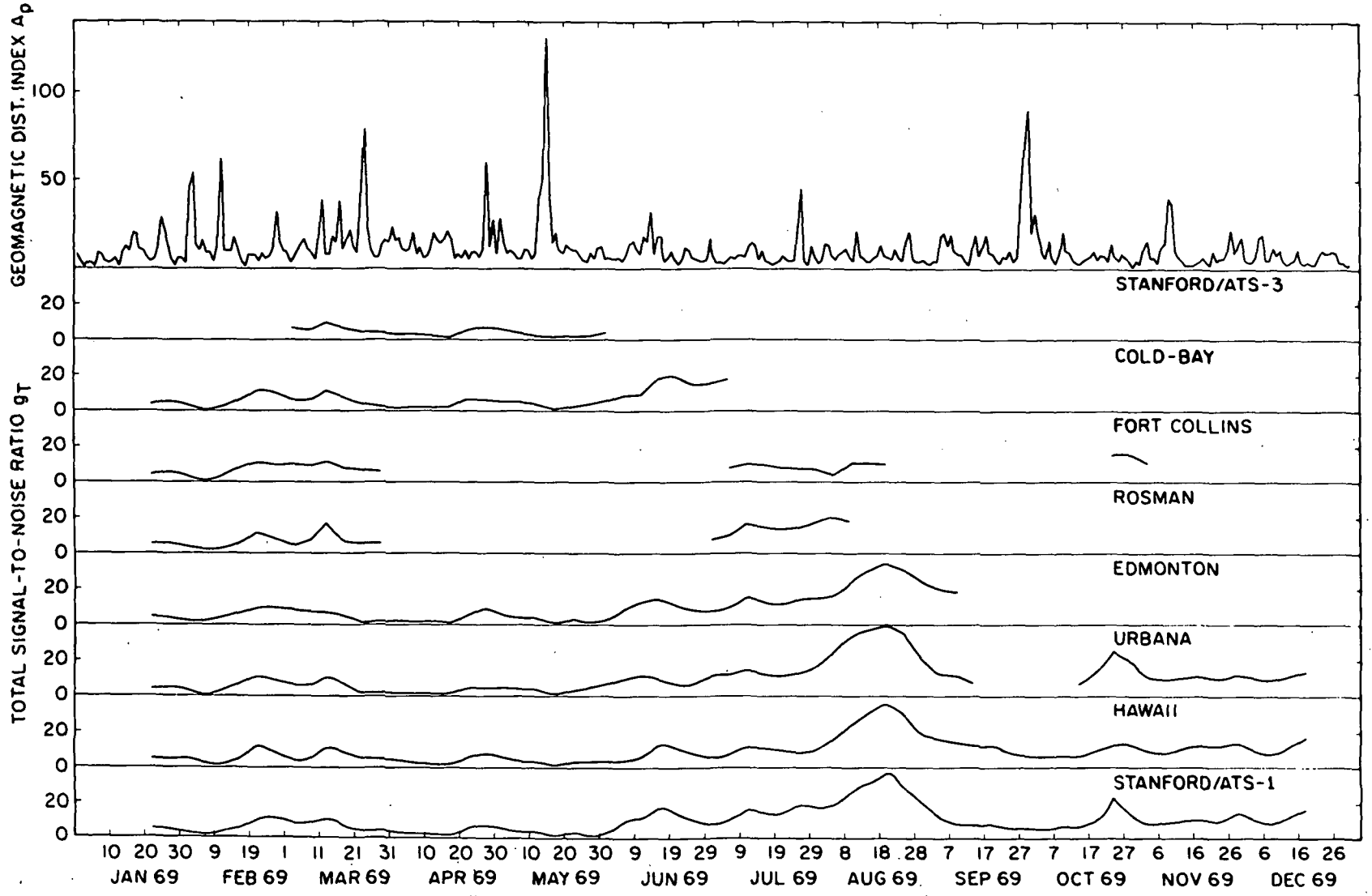

Fig. 5.3. Variations of the geomagnetic disturbance index, A_p, and of the total signal-to-noise ratio g_T, corresponding to stations at Stanford, Hawaii, Cold Bay, Fort Collins, Rosman, Edmonton, and Urbana, during the year of 1969.

fluctuation with 27-days period and if the magnetic activity is low.

It can be seen in those figures that the delay hovers between 1.8 and 2.1 days during the period of large signal-to-noise ratio corresponding to the autumnal equinox.

The long term average of the solar flux during 1969 was close to 150 units. The delay found from theoretical considerations for that solar activity, Table 3 (Chapter 4), was 1.8 days which is in agreement with the observed values in Figures (5.4a) and (5.4b).

Thus, from the above observations, it becomes apparent that under appropriate conditions it is possible to predict the ionospheric delay with respect to the solar forcing function; however, the prediction of the ionospheric sensitivity depends on additional factors not included in the model developed in this work, as can be seen by an examination of Figure (5.5). This figure represents the electron content behavior at three different stations during the favorable period of 22 May 1969 to 29 September 1969. During this period, as we have pointed out above, the solar radio noise varied in an almost sinusoidal fashion and four 27-day cycles are clearly seen. One would expect that the electron content fluctuation at the different stations would be proportional to the corresponding solar radio noise fluctuations. This however, is not the case. The first and largest cycle of solar radio noise produced a relatively small effect in the ionosphere, especially at Urbana and Hawaii. An examination of the fluctuations of the 304 Å He II line during this period, helps to partially explain the discrepancy observed: It appears

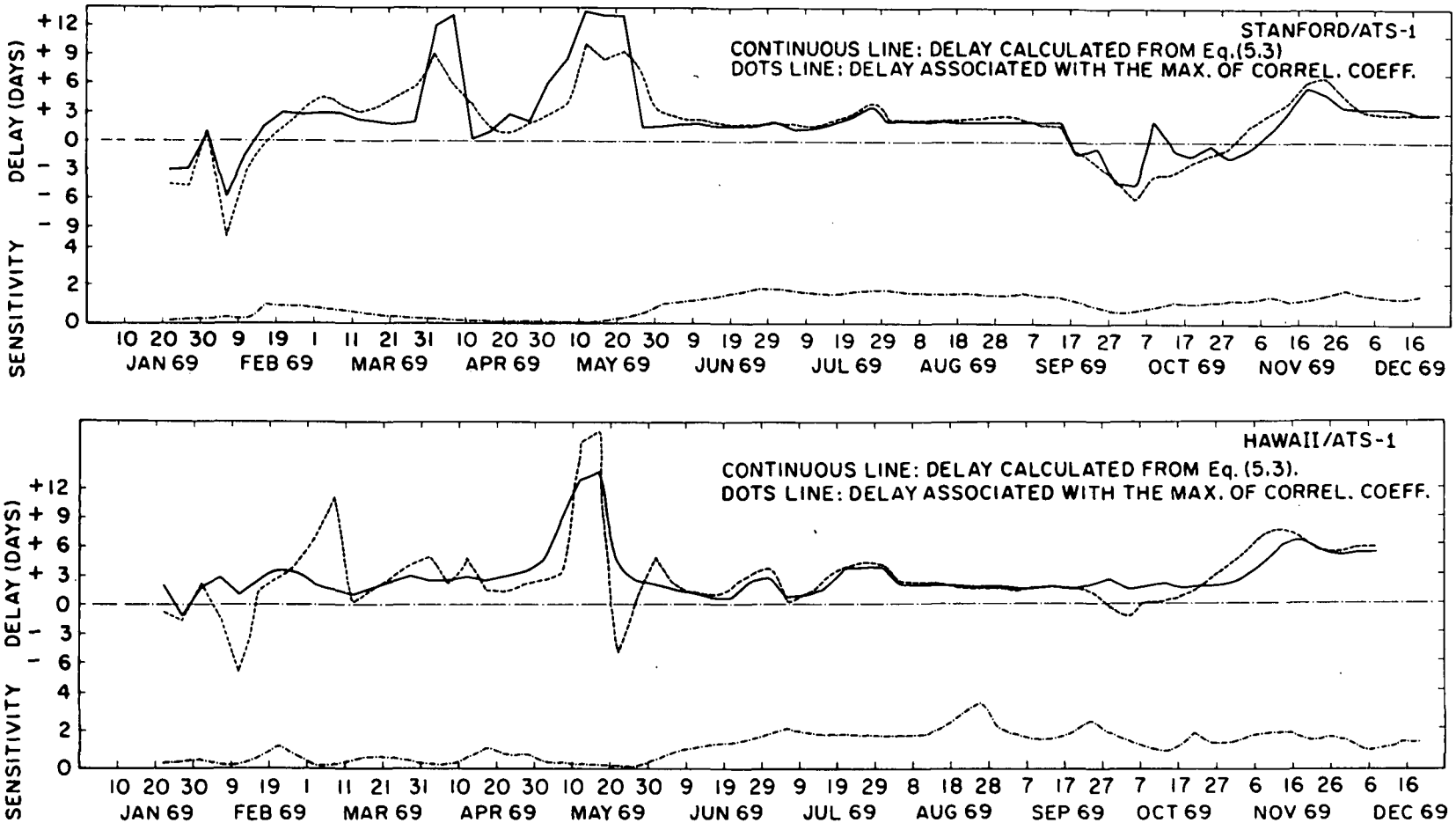

Fig. 5.4a and 5.4b. Plots of delays and sensitivities corresponding to Stanford ATS-1 and Hawaii stations, during the year of 1969.

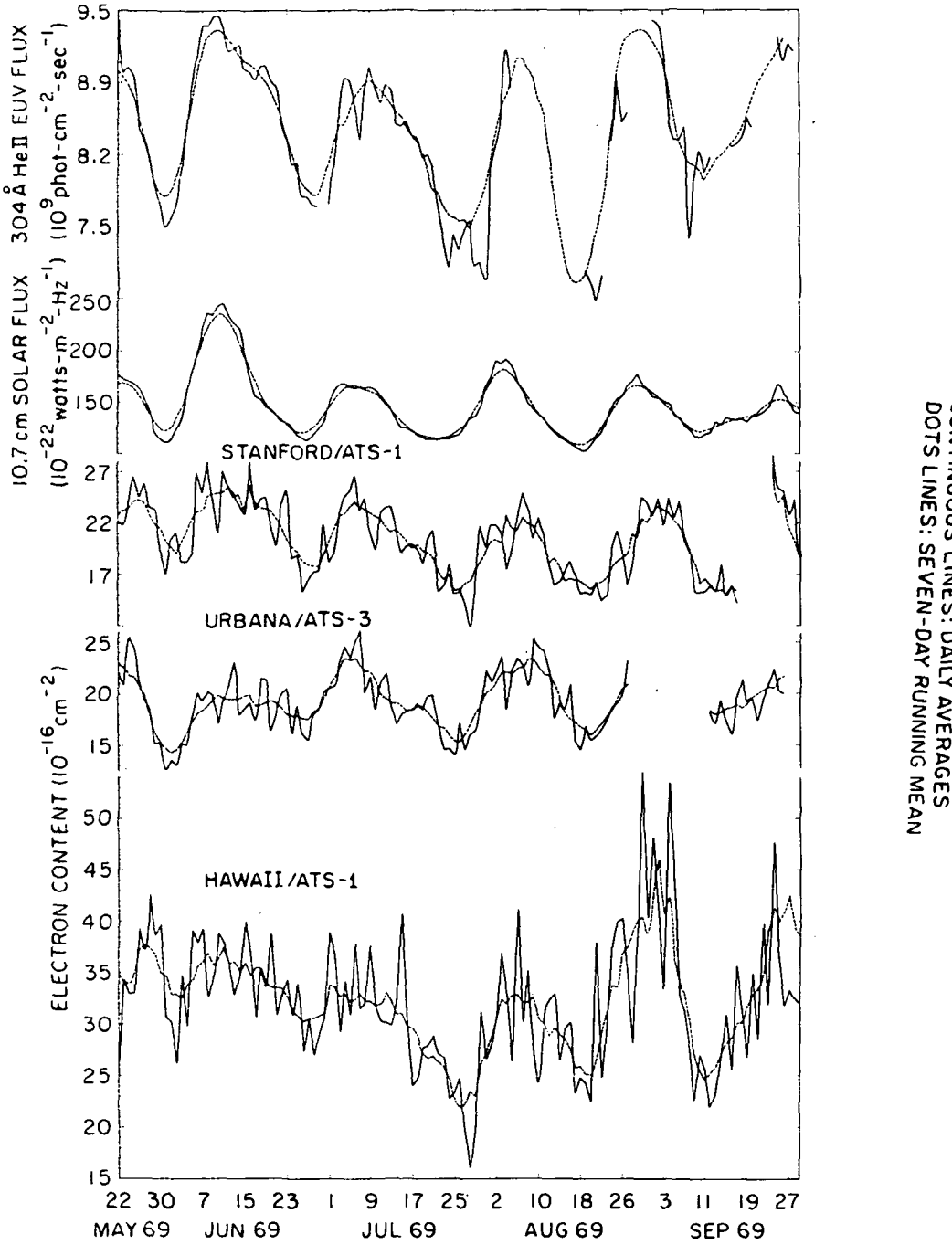

Fig. 5.5. Variations of the 304 Å HeII, the 10.7 cm solar flux and of the electron content at Stanford ATS-1, Urbana, and Hawaii stations during the favorable period of 22 May 1969 to 29 September 1969.

that the radio flux did during the first cycle depart considerably from the behavior of the EUV, showing an exagerated amplitude.

The difference of behavior of the ionosphere at various places, in response to a given fluctuation in solar radiation can obviously only be explained by differences in local conditions, differences which have not been taken into account in the theoretical study made in this work. It was shown in Chapter 2 that in the absence of the wind feed-back mechanism the electron content sensitivity is expected to be less than 1, and in the more complete investigation in Chapters 3 and 4, it was shown that the inclusion of the feed-back mechanism will cause the sensitivity to become larger than unity. The observed sensitivities at Stanford and Hawaii during the period in question, are all larger than one suggesting that indeed, the wind feed-back mechanism is present.

CHAPTER 6

CONCLUSIONS

The general purpose of the present work was to examine the dynamic interaction between electron content and solar flux, and in particular to determine the ionospheric response to the 27-day variations of the solar flux, i.e., the sensitivity and delay corresponding to the electron content.

The dependence of the level of solar activity to changes in the ionospheric response has been theoretically analyzed for both the case in which the action of neutral winds on the F2 layer is disregarded and for that in which the wind effect is considered. The comparison of the results leads to the conclusion that neutral winds play a dominant role in the mentioned dependency. The reason lies in the positive feed-back mechanism discussed in Chapter 3.

A technique has been developed in Chapter 2 for solving the continuity equation for the daily average of the electron content when the action of neutral winds is disregarded. The technique consists in taking daily averages of the continuity equation, written in terms of the electron content. This technique leads to two important simplifications: the integrated transport term cancels out and the magnitude of the time-derivative of the daily average of the electron content is negligible when compared with the magnitude of the other terms. From the simplified version of the continuity equation it was possible to derive the sensitivity and delay corresponding to the electron content in terms of the solar input and of the daily average of the weighted mean of the recombination coefficient.

By adopting a model for the neutral atmosphere and using an empirical expression relating the neutral temperature profile to the solar flux, it was possible to express both delay and sensitivity in terms of only the solar input.

When the action of neutral winds was considered the continuity equation of ionization and the equation of motion of the neutral atmosphere were solved for the ionization and the neutral wind velocity profiles in a self-consistent fashion. The simplifications made in both equations include:

a) The electron content measured at 1400 L.T. was taken as an index of the daily average of the electron content. This simplification allowed considering the continuity equation under steady-state conditions.

b) The viscosity effect on the neutral wind velocity profile was considered only as a boundary condition. This simplification made it possible to convert the two differential equations of the horizontal components of the neutral wind velocity into a pair of algebraic equations, the solution of which was carried out analytically.

The technique for integrating the reduced pair of equations resulting from the above simplifications was discussed in detail in Chapter 4.

With the same model of the neutral atmosphere adopted in Chapter 2 and the same empirical expression relating the neutral temperature profile with the solar flux, it was possible to develop an elaborated set of formulae which allowed the calculation of all parameters involved in

the equations to be integrated in terms of only the solar input. Therefore, the only datum required to feed the computer program, prepared for integrating the pair of differencial equations, is the solar flux.

A sinusoidal solar input with 27-days period applied at the input of the non-linear system proposed in Chapter 3 was quantized, i.e., it was considered as a series of step functions. At the output of the system one finds a wave-form, representing the electron content, from which it was possible to derive the corresponding sensitivity and delay. Furthermore, with the purpose of saving computer time, a major simplification was done consisting in linearizing the system. However, the results did not show much sensitivity to this simplification.

The delays in the ionospheric response decrease with increasing solar activity in both the "no wind" model and the one in which wind effects are considered. In this latter case the delays are somewhat larger.

The "no wind" model predicts a sensitivity smaller than unity while the effect of the wind causes this sensitivity to be larger than one, i.e., the relative fluctuations in electron content become larger than those in solar radio flux. With no winds, an increase in solar activity levels leads to an increase in sensitivity, the opposite occurring in the model that takes winds into account.

The experimental verification of the theoretical results described above is difficult in view of the presence of a number of other effects not included in the model. Such effects were treated as noise while the response of the ionosphere to the fluctuation of the solar flux was

taken as the desired signal. The observed data were examined only when the "signal-to-noise ratio" was sufficiently high.

This requires the presence of two conditions:

a) Solar flux fluctuations with sufficient amplitude.

b) Low amplitude of the perturbations.

Condition a) occurs, in general, during geomagnetically quiet periods.

When the above conditions coexist, the ionosphere responds in approximately the manner predicted by the model described in Chapter 4:

- The observed delays are of the magnitude predicted by the theory.
- The sensitivities are larger than one.

REFERENCES

Abur-Robb, M.F.K., "Combined world-wide neutral air wind and electrodynamic drift effects on the F2-layer", Planet. Space Sci., 17, 1269, 1969.

Almeida, O.G., "VHF/UHF Technique for the determination of the columnar electron contents of the plasmasphere and of the protonosphere using geostationary satellite transmissions: Observations during magnetic storms", Tech. Rept. No. 14, SU-SEL-72-019, Stanford University, Stanford, California, 1972.

Amayenc, P., and G. Vasseur, "Neutral winds deduced from incoherent scatter observations and their theoretical interpretation", J. Atmos. Terr. Phys., 34, 351, 1972.

Bates, D.R., "Some problems concerning the terrestrial atmosphere above about 100 km level", Proc. Roy. Soc., A253, 651, 1959.

Bhonsle, R.V., A.V. da Rosa, and O.K. Garriott, "Measurements of the total electron content and the equivalent slab thickness of the mid-latitude ionosphere", Radio Science, 69D, 1965.

Bourdeau, R.E., S. Chandra, and W.M. Neupert, "Time correlation of extreme ultraviolet radiation and thermospheric temperature", J. Geophys. Res., 69, 6531, 1964.

Bramley, E.N., and Margaret Young, "Winds and electromagnetic drifts in the equatorial F2-region", J. Atmos. Terr. Phys., 30, 99, 1968.

Carpenter, L.A., and S.A. Bowhill, "Investigation of the physics of dynamical processes in the topside F-region", Aeronomy Report No. 44, University of Illinois, Urbana, Illinois, Sept. 1971.

Chandra, S., and B.V. Krishnamurthy, "The response of the upper atmospheric temperature to changes in solar EUV radiation and geomagnetic activity", Planet. Space Sci., 16, 231, 1968.

Chapman, S., Nuovo Cimento, 4, 1385, 1956.

CIRA 1965: Cospar International Reference Atmosphere: 1965, North-Holland Publishing Co., Amsterdam, 1965.

Dalgarno, A., and F.J. Smith, "The thermal conductivity and viscosity of atomic oxygen", Planet. Space Sci., 9, 1, 1962.

da Rosa, A.V., and O.K. Garriott, "Protonospheric electron concentration profiles", Final Report, Radioscience Laboratory, Stanford University, Stanford, California, 1969.

da Rosa, A.V., H. Waldman, J. Bendito, and O.K. Garriott, "Response of the ionospheric electron content to fluctuations in solar activity", J. Atmos. Terr. Phys., in press, 1973.

Evans, J.V., "Observations of the F-region vertical velocities at Millstone Hill, 2. Evidence for fluxes into and out of the protonosphere", Radio Science, 6, 843, 1971.

Evans, J.V., "Ionospheric movements measured by incoherent scatter: A review", J. Atmos. Terr. Phys., 34, 175, 1972.

Garriott, O.K., A.V. da Rosa, and M.J. Davis, "Enhancement of ionizing radiation during a solar flare", Solar Physics, 8, 226, 1969.

Garriott, O.K., A.V. da Rosa, and W.J. Ross, "Electron content obtained from Faraday rotation and phase-path length variations", J. Atmos. Terr. Phys., 32, 705, 1970.

Geisler, J.E., "Atmospheric winds in the middle latitude F-region", J. Atmos. Terr. Phys., 28, 703, 1966.

Geisler, J.E., "A numerical study of the wind system in the middle thermosphere", J. Atmos. Terr. Phys., 29, 1469, 1967.

Hays, W.L., Statistics for Psychologists, Holt, Rinehart, and Wiston ed. Co., 1965.

Herman, J.R., and S. Chandra, "The influence of varying solar flux on ionospheric temperatures and densities: A theoretical study", Planet. Space Sci., 17, 815, 1969.

Hinteregger, H.E., L.A. Hall, and G. Schmidtke, "Solar XUV radiation and neutral particle distribution in July 1963 thermosphere", Space Res., V, North-Holland Publishing Co., Amsterdam, 1175, 1965.

Jacchia, L.G., "The temperature above the thermopause", Space Res., V, 1152, 1965.

Jacchia, L.G., "Static diffusion models of the upper atmosphere with empirical temperature profiles", Smith. Contr. Astrophysics, 8, N-9, 1965.

King, J.W., and H. Kohl, "Upper atmospheric winds and ionospheric drifts caused by neutral air pressure gradients", Nature 4985, 699, 1965.

Kohl, H., and J.W. King, "Atmospheric winds between 100 and 700 km and their effects on the ionosphere", J. Atmos. Terr. Phys., 29, 1045, 1967.

Nisbet, J.S., "On the construction and use of a simple ionospheric model", Radio Science, 6, 437, 1971.

Park, C.G., "Whistler observations of the interchange of ionization between the ionosphere and the protonosphere", J. Geophys. Res., 75, 4249, 1970.

Ratcliffe, J.A., and K. Weekes, "The Ionosphere", in Physics of the Upper Atmosphere, edited by J.A. Ratcliffe, Academic Press, New York and London, 377, 1960.

Rishbeth, H., "On explaining the behavior of the ionospheric region", Reviews of Geophysics, 6, 33, 1968.

Rishbeth, H., "The effect of winds on the ionospheric F2-peak", J. Atmos. Terr. Phys., 29, 225, 1968.

Rishbeth, H., "Thermospheric winds and the F-region: A review", J. Atmos. Terr. Phys., 34, 1, 1972.

Rishbeth, H., and D.W. Barron, Equilibrium electron distributions in the ionospheriv F2-layer", J. Atmos. Terr. Phys., 18, 234, 1960.

Stubbe, P., "Simultaneous solution of the time dependent coupled continuity equations, heat conduction equations, and equations of motion for a system consisting of a neutral gas, an electron gas, and a four component ion gas", J. Atmos. Terr. Phys., 32, 865, 1970.

Stubbe, P., and S. Chandra, "The effect of electric fields on the F-region behavior as compared with neutral wind effects", J. Atmos. Terr. Phys., 32, 1909, 1970.

Thomas, G.E., and B.K. Ching, "Upper atmospheric response to transient heating", J. Geophys. Res., 74, 1796, 1969.

Thomas, G.E., and B.K. Ching, "A theoretical study of the 27-day variation of upper-atmospheric temperature", Planet. Space Sci., 17, 1737, 1969.

Vasseur, G., "Dynamics of the F-region observed with Thomson-scatter. I. Atmospheric circulation and neutral winds", J. Atmos. Terr. Phys., 31, 397, 1969.

Waldman, H., "The coupling between the ionosphere and the protonosphere and its implications on the long-term variations of ionospheric electron content", Tech. Rept. No. 13, SU-SEL-71-048, Stanford University, 1971.

Whitten, R.C., and I.G. Poppof, Fundamentals of Aeronomy, John Wiley & Sons, Inc., New York, 282, 1971.